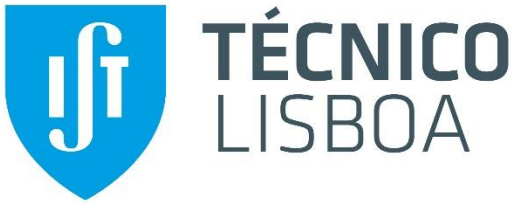

Windsurf Fin- Numerical and Experimental Analysis of Ultimate Strength

Francisco de Albuquerque Marcão Ramos do Nascimento

Thesis to obtain the Master Degree in

Naval Architecture and Marine Engineering

Supervisor: Prof. Yordan Garbatov

Co-supervisor: Dr Leigh Sutherland

Examination Committee

Chairperson: Prof. Carlos Guedes Soares

Member of the Committee: Prof. Yordan Garbatov

Member of the Committee: Prof. Ângelo Teixeira

July 2017

"All truths are easy to understand once they are discovered;
the point is to discover them"

Galileo Galilei

This page was intentionally left in blank.

Acknowledges

First, I want to show gratitude to my supervisors, Prof. Yordan Garbatov and Dr. Leigh Sutherland. From the first minute for all the knowledge, constant availability, motivation and continuous guidance during all the project. It was a pleasure to learn and advance this project under their supervision

To all my friends and colleagues that made this possible, helping during Marine Engineering and Naval Architecture course, companions of good adventures. Without all of them, it was not possible to reach this point, achieving all the objectives with such a great joy. Thank you for everything.

To the company, F-Hot for the possibility to develop this project and thank you for all the necessary support.

To my family, especially to my mother, which made this possible, allowing me to go under this journey with a lot of patience and trust in every moment, and for every sacrifice during all these years.

Last, but not the least, to Margarida, with an unconditional support in every moment, putting all her strengths to help me to complete every single stage during this great battle. Thanks MR.

This page was intentionally left in blank.

Resumo

O objectivo deste trabalho é analisar numericamente e experimentalmente a resistência última de uma quilha de windsurf produzida em materiais compósitos. Um modelo de elementos finitos é desenvolvido e posteriormente validado por uma experiência com um modelo à escala real. A análise de elementos finitos é realizada no programa ANSYS. A estrutura da quilha é analisada, tanto no domínio linear como não linear quando sujeita a cargas pontuais, aplicadas em diferentes localizações da estrutura, identificando a evolução das tensões e consequentes deformações. Para além do modelo numérico, é também analisada a estrutura no laboratório, reproduzindo as cargas simuladas no computacionalmente. Os resultados numéricos são analisados, comparados e consequentemente calibrados com os valores obtidos experimentalmente. Para determinar o estágio de falha, o critério de falha Tsai-Wu é implementado, que prevê a ocorrência ou não de falha, independentemente do modo em que essa falha é aplicada. Também são aplicados os critérios de Tensão Máxima e de Extensão Máxima de forma a prever a falha última da quilha.

Palavras-Chave: ANSYS, Materiais Compósitos, Método de Elementos Finitos, Resistência Última, Tsai-Wu

This page was intentionally left in blank.

Abstract

The objective of this work is to analyze numerically and experimentally the ultimate strength of a windsurf fin, produced in composite materials. A FE model is developed and validated by a real scale-experiment. The FE analysis is performed using the commercial software ANSYS. The fin structure is analyzed, both in the linear and non-linear domain when subjected to remote load, applied at different locations of the structure, identifying the evolution of the stresses and the consequent deformation. Beyond the numerical model, it is also analyzed the structure in the laboratory, reproducing the load used in the computational analysis. The output of the numerical analysis is compared to experimental one and calibrated. To determine de fin's stage of failure the Tsai-Wu failure criteria, which predicts only if exists or not breaks, independently the mode which the fin breaks is employed. Were also applied the Maximum Stress Criteria and the Maximum Strain Criteria to have predictions of the complete break of the fin.

Key-Words: ANSYS, Composite Materials, Finite Element Method, Tsai-Wu, Ultimate Strength

This page was intentionally left in blank.

Table of Content

List of Figures

List of Tables

Glossary

FVF- Fibre Volume Fraction

FWF- Fibre Weight Fraction

FEM- Finite Element Method

FEA- Finite Element Analysis

3-D - Three Dimensional

ANSYS- Computational Software used to Create the Model

CAD- Computer-Aided Design

CENTEC- Centro de Engenharia e Tecnologia Naval e Oceânica

List of Symbols

v_c - Volume of Composite

v_f - Volume of Fibre

v_m- Volume of Matrix

V_f - Volume Fraction of Fibre

V_m- Volume Fraction of Matrix

w_c - Weight of Composite

w_f - Weight of Fibre

w_m- Weight of Matrix

W_f - Weight Fraction of Fibre

W_m- Weight Fraction of Matrix

ρ_c- Density of Composite

ρ_f- Density of Fibre

ρ_c- Density of Matrix

m_f- Mass of Fibre

m_m- Mass of Matrix

t- thickness

φ_i- Field Variable at Node i

Ni- Interpolation Functions (Shape Functions) at Node i

Fi- second rank tensors

Fij- fourth rank tensors

σ_{ij} - Stress in Direction ij

X_t - Tension in Direction of Fibre

X_c - Compression in Direction of Fibre

Y_t - Tension Transverse to Direction of Fibre

Y_c - Compression Transverse to Direction of Fibre

S- Shear

Cij- Material Constants (Stiffness)

$\boldsymbol{\varepsilon}_{ij}$- Strain in Direction ij

Sij- Compliances

x, y, z- Axes Directions

E- Young Modulus

ν- Poisson Ratio

G- Shear Modulus

$\boldsymbol{\sigma}_{x\,(T)}$, $\boldsymbol{\sigma}_{y\,(T)}$, $\boldsymbol{\sigma}_{z\,(T)}$- Orthotropic Stress Limits in Tension

$\boldsymbol{\sigma}_{x\,(C)}$, $\boldsymbol{\sigma}_{y\,(C)}$, $\boldsymbol{\sigma}_{z\,(C)}$- Orthotropic Stress Limits in Compression

τ_{xy}, τ_{yz}, τ_{xz} -Orthotropic Stress Limit (Shear)

$\varepsilon_{x\,(T)}$ $\varepsilon_{y\,(T)}$ $\varepsilon_{z\,(T)}$ - Orthotropic Strain Limits in Tension

$\varepsilon_{x\,(C)}$ $\varepsilon_{y\,(C)}$ $\varepsilon_{z\,(C)}$ - Orthotropic Strain Limits in Compression

ε_{xy}, ε_{yz} and ε_{xz}- Orthotropic Strain Limits (Shear)

1 Introduction

1.1 Motivation

The maritime market choice for composite is more and more attractive. It is now possible to construct composite structures which performs better than the metal ones, wherever we talk in terms of weight, strength or cost. To achieve this, it requires a good control of quality. It is also important that the designer and producer have a knowledge of fibre reinforced plastics (FRP) composite materials and associated mechanics. Composites offer the prospect of weight saving and low maintenance, as well as being non-magnetic. These advantages put the composite materials far ahead, when the shipyards must decide whether go to metallic or composite materi1als.

As materials and building practices improve, it is not unreasonable to consider composite construction for vessels up to 100 meters. Although design principles for ship structures and composite materials used in aerospace structures are mature as individual disciplines, procedures for combining the technologies are at an infancy (Greene 1999).

Creation of valid numerical models is the only possible way to predict the complex behavior of the materials, due to their anisotropic properties and multifaceted internal interactions. The finite element method analysis is an important tool in this sector. With the advance of powerful finite element (FE) models, the accuracy of the predictions gets higher and higher, enabling the shipyards to construct with more confidence and reducing the margin of error. The nautical sports sector is one of the areas where more investment is made to obtain better results, due to its high level of competition and the constant necessity of keep in the vanguard of the expertise.

The application of finite element method to study the structural response of windsurf fins is still undeveloped, making the margin of progression a motivation to address this area. The sector is reaching a point where the expertise of the shipyards requires numerical support to advance, to improve the performance and obtain better results. The know-how is getting overcome by the finite element application and in the nautical sports area this is getting more evident with the consequent introduction of FEM analysis in the design of every part or boat of high level of competition. Windsurf area is not an exception, and the preliminary improvements are being obtained by the leading companies of the sector, showing the necessity of winning every competition, wherever talking about world championships or even the Olympics where this sport participates from 1984.

The windsurfing fin is one of the most important pieces in this sport. It is the board's pivot point, and plays a major role in the board's manoeuvrability. To understand this, it is necessary to think the fin as a wing in the water that is the same on both sides. As any wing, the fin is designed to allow pressure to flow from the side, and divert the pressure into forward thrust and lift (Raby 2011).

To reduce trial and error fabrication processes, the implementation of Finite Element Method is an essential tool. The capacity of easily changing internal properties, shapes or other important aspects, which can be tested and help to predict the structural response to the applied loads. To builders like F-Hot, who produces fins to world champions, it is essential to understand the structural behavior under hydrodynamic pressure loads during sailing. Due to the complex nature of the fin's structure with its stiffeners, plies of carbon and glass at various orientations, it would be difficult to predict the twist and flexure of the fin using standard hand calculations. The finite element model allows the user to easily modify the composite lay-up of the fin to reach the desired structural characteristics, achieving better results quicker and with less effort.

The Finite Element Method has become the most powerful instrument in structural analysis, allowing to analyze the strength of highly complex structures, wherever this complexity comes from its size or questions about the difficulty to predict of the response of composite materials.

Therefore, the scope of this work is to analyze a windsurf fin studying its ultimate strength, through a numerical model in FEM and experimentally in the laboratory of a real-scale fin.

1.2 Objectives

The principal objective is to create a numerical model of a windsurf fin, analyzing its ultimate strength. This numerical model is to be calibrated with the data obtained in the laboratory, where a real-scale model is to be tested.

The tests are going to be settled in two ways: Numerically, where the model is created to be analyzed in terms of stresses and deformations, applying after a failure criterion for composite materials; and experimentally, where the fin is to be tested only in the linear-elastic domain, where the resulting values are going to be used in the numerical model to calibrate it, correcting the initial differences of the structural response after applying remote loads at different points of the structure.

This work is an important first step to further developments about the windsurf fin, allowing future FEM projects to start a step ahead.

2 State of the Art

2.1 Composite in Maritime Sports

The use of FRP in maritime structures has been increasing since early 1950's. Originally, it was only used for small crafts, like lifeboats and pleasure craft. Over the years, this tendency has changed, as massive structures made in composites with hundreds of tones are now regularly used. The volume and number of applications of composite materials have grown steadily, penetrating and conquering new markets persistently.

There is an enormous market to be won in the offshore oil industry, where the fire and blast protection of emergency shut down valves, personnel shelters, accommodation modules and piping and decking can derive from the fire barrier that FRP provides besides being weight-saving over steel (Shenoi and Wellicome 1993).

Particularly in the nautical sports, the use of composite materials in marine engineering has been growing very fast. The windsurf is a good example of it, with a fast development in equipment and in the material selection. Lead constructors and designers are interested in developing new forms of skegs and fins. They realized that fins are as important as boards and sails. However, the importance of the fin was underestimated. Nowadays it is known that the fin resists to nearly all side force, which is made from the sails and its role is to produce a lifting force and counteract the side force.

The speed of windsurfing depends on a reduction of the drag force of the fin. Without the fin, it would not be possible to sail, the board would float with the drift. The lifting force, which is made by the fin, is between 300 N and 600 and drag force vary between 20 N and 50 N (and it is approximately one-sixth of the total drag). For now, the development of fin shapes and materials are in very advanced stage of evolution, the importance of the fin is well known. However, it seems that without more researches and changes in design and used materials, it is not possible to improve the functioning of the fin (Nowakowska et al. 2011).

Figure 2.1- Global Model of Windsurf Equipment

As it can be seen in the Figure 2.1, the windsurf equipment is composed of three major parts: the mast and sail, the board and the fin. The last one is the one that is going to be the objective of analysis in this dissertation. There are different types of fins to adjust better to the area, that the rider is competing, commonly known as “wave”, “slalom” and “course racing”. The first one is where the board is used to ride and jump waves breaking the beach. This type of windsurf is very demanding for the fins, with sudden changes of direction and a lot of impacts, requiring good strength values for this fin. “Slalom” sailing requires a lot of speed, making the reduction of drag and the increase in lift important requirements, when designing the fin. The “course” should be a more balanced fin and perform well on all points of sailing (Sutherland 1993).

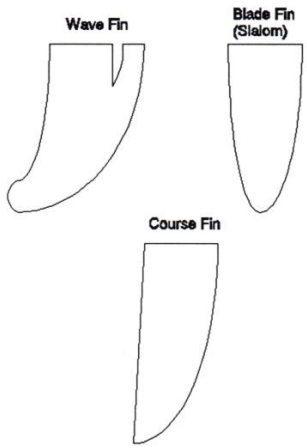

Figure 2.2- Types of Fins (Sutherland 1993)

2.2 Structure of Dissertation

To reach the main objective of analyzing numerically and experimentally the windsurf fin, there were intermediate steps, that were need to be done. In this way, the work flow can be resumed in the graphic bellow:

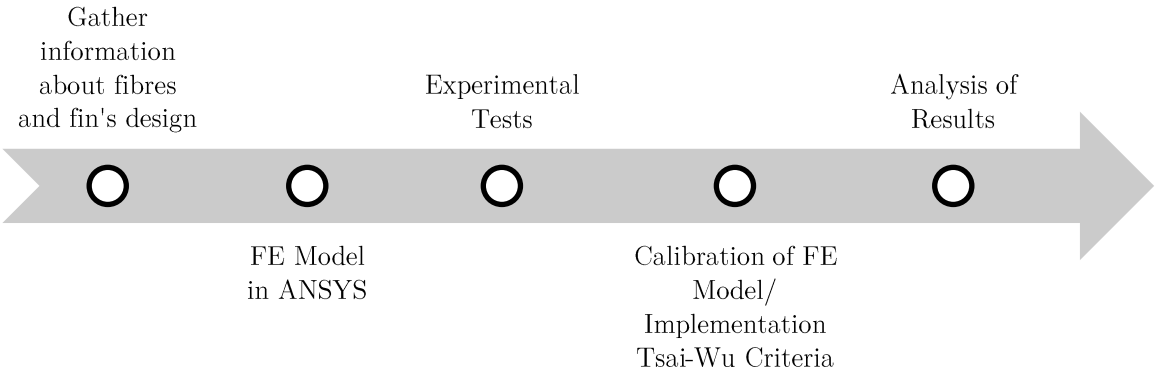

Figure 2.3- Working Flow

The research about the information needed to achieve he objectives purposed was made during the process. A bibliographic review is going to be made here, explaining why they were used in this dissertation.

The nautical sports sector is highly competitive. The major shipyards keep their knowledge with them, using the information given by years of try and error, with no support of numerical models. To reach main goals of this project, it was important to gather the information related with the material properties, the failure criterion values that can be used and some relevant structural data to make the necessary experimental tasks.

Shenoi and Wellicome (1993) are one of the major sources of information about the behavior, constituent equations and other important relations in how the materials should be designed and what values are usual in the fabrication of maritime structures. Some other authors, like Barbero (2010), published important books especially for designing, not structures but the materials itself, or laminates, giving more focus on the materials properties. The improvement of the guidelines to develop and process composites has had continuous support from the aeronautics, where the budgets are higher and where the margin of error is smaller. In this way Gregg Bogucki, William McCarvill, Stephen Ward (2003) created a document for the United States government, where a set of guidelines of constructions, designing and validations of fabrications processes and methods can be observed. The big fabrication companies of these materials are one of the major developers of composites and, specially, one of the biggest responsible for publish the material properties, that help to make the calculations to validate the expertise used in the shipyards and, being possible to create FE models that, more and more, are getting closer to the reality (although errors are still bigger than metallic or other isotropic materials). Gurit Holding AG (2000) and Hexcel (2013) are examples of it, with the creation of complete catalogues where the material properties are established. The shipbuilding industry has grown in this sector, making the composite boats a high percentage of vessels, especially in the pleasure and small fast boats, which have increased in size over the years. Greene (1999) is a good example of how some classical theories in terms of stresses and responses can be applied also to composite materials, with the respective changes and considerations. This makes it possible to predict the behavior with the characterization of the classical theories in composite structures.

With the evolution of computers, the importance of trying to predict the behavior of structures has become essential, especially with materials with a very unpredictable behavior such as composite materials. Although the models cannot be completely trustable, due to the complexity of the internal arrangements of the layered structures, they can give an estimate and, with good safety margins, it is much better than some rough calculations. The basis of software's like ANSYS are the mathematical expressions and demonstrations expressed by Matthews et al. (2000). The connections between a finite element method software's like ANSYS with composite materials are described by Barbero (2008a) and (2008b), unfolding the equations and theory beyond the computational processes. One of the important sources of material properties was from Miller (1991), which is a not publish report about composite material properties. This kind of related information is also developed by the software companies who are dealing with more and more competition, and releasing new versions with updates tools, with a growing focus on the composite

analysis. Ansys Inc. (2013) is one of the biggest players in this market and they create manuals to help in this complex task to generate the best possible models

After researching about the composites and how to implement them using the finite element method, it was important to search for the structural response of this special materials, the relation with the classical theories and understand what kind of assumptions should be made. Timoshenko (1965) and Gere and Timoshenko (1991) reported explanations about the classical responses to concentrated loads, like the ones that are going to be tested in the fin (knowing that anisotropic or even orthotropic materials response very differently). Knowing these particularities of orthotropic materials, studies of Savoia and Tullini (1996) and Silvestre and Camotim (2002) were used to compare the beam theory with composite materials. In the field of the beam theory in composites, Wim Van Paepegem (2002) analyzed and computed the equations that are applied to composite materials, adjusting the classical equations to the particularities of the non-isotropic materials. Fagg (1997) made a study that includes comparisons between real tests and the values obtained with the application of the beam theories, showing important factors and points that should be compared when making numerical and experimental analysis. Kelly (2015) studied the simplifications of the orthotropic materials, applying the plain stress case to anisotropic materials and the relation between their strains and stresses.

Understanding that the windsurf fins are not to be used after the first failure, it was selected a criterion of failure, that would indicate the signal of failure in the first instant, independently the mode that it happens. Tsai and Wu (1971) presented a criterion, that indicates the first failure, independently the mode. Pinho (2005) and Camanho (2002) studied other norms to define the failure moment, establishing the most interesting failure criteria composites, specifying each advantages and disadvantages. This last report was also used to get information about criteria of maximum stress and strain of the fibres, which were used to make some predictions about the ultimate failure.

This page was intentionally left in blank.

3 Theoretical Background

3.1 Composite Materials

Composite materials are composed of at least two elements working together to produce material properties that are different to the properties of those elements on their own. Most composites are made up of a bulk material (the 'matrix'), and a reinforcement of some kind, usually in fibre form. Polymer matrix composites (PMC's) combine a resin system and reinforcing fibres. One of the advantages of the composite is that two or more materials could be combined to take advantage of the good characteristics of each of the materials (Rusmee 2014).

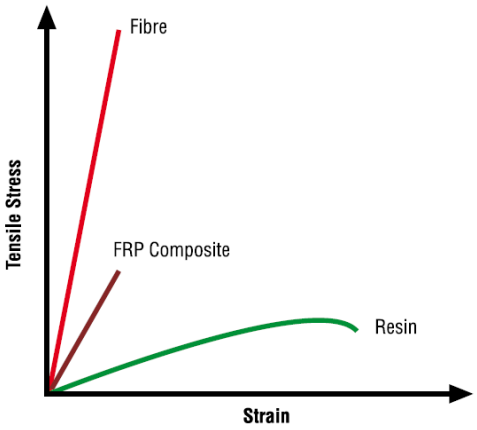

Figure 3.1- Generic Stress-Strain of Fibre, Resin and the final Composite (Gurit Holding AG 2000)

Generically, the properties of the composite are set (by this order) by:

1. Properties of the fibre,
2. Properties of the resin,
3. Ratio between fibre and resin (Fibre Volume Fraction- FVF),
4. Geometry and orientation of the fibres.

Although the application of the composites varies a lot from shipyard to shipyard, the common hand lay-up process as widely used in the boat industry, the limit for FVF is between 30 to 40%. The aerospace industry uses higher values, reaching up to 70% of fibre volume fractions (Gurit Holding AG 2000).

There are various types of composites. To understand this, it is used a scheme as presented in Figure 3.2 to resume the classification of the composites.

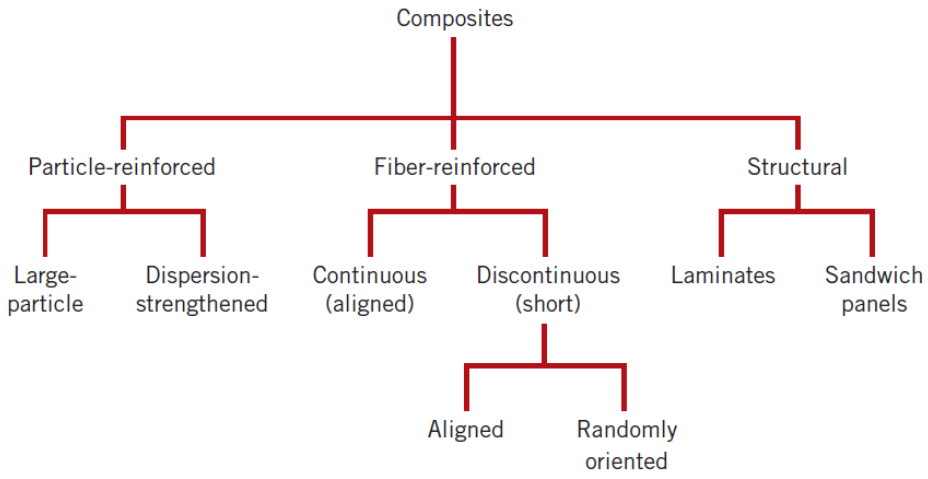

Figure 3.2- Classification scheme for the various composites types (Callister and Rethwisch 2007)

In the present study, a fibre-reinforced composite was used, so it is the only type that is going to be discussed.

To better understand how the composites work, the resulting composite is made up in a laminate, stacking up plies (from the same material or not), that can be in different orientations, as seen in Figure 3.3.

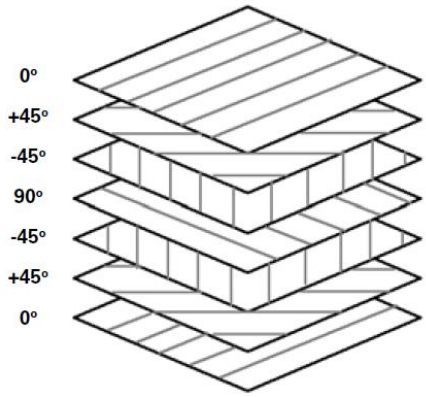

Figure 3.3- Laminate Notation (Gurit Holding AG 2000)

In polymeric composite terms, a fabric is defined as a manufactured assembly of long fibres. The fabric types depend on the orientation of the fibres used and the construction methods to hold the fibres together

In this way, there are some fabric types, although in this dissertation are only going to be explained the first two because are the ones are going to be used (Gurit Holding AG 2000).

1. Unidirectional (UD),

   Are fabrics with fibres in only one direction, gathered by mechanical or chemical stitching. The main characteristics are:

   - High tensile and compression strengths in the fibre direction, due to high quantity of fibres in the fibre direction and due to lack of waviness,
   - Low tensile and compression strengths in the transverse direction (Bureau Veritas 2012).

2. Woven Roving (WR),

   Are made from two sets of fibres crisscrossing, which forms a right angle. The one in the weaving direction is named warp, the other one is named weft. The weaving consists of repeating a basic interlaced sequence between rovings, given the name of this sequence, basic weave. There are four main weave families used in shipbuilding. Again, only the first will be explicated because it is only that will be considerate (Bureau Veritas 2012).

   - Plains,

     Each weft fibre passes alternatively under and over each warp fibre. This type of fabric is relatively difficult to drape due to its high stability. The fibres are strongly crisscrossed (high waviness)

   - Baskets,
   - Twills,
   - Satins.

3. Chopped Strand Mats (CSM),
4. Combined Fabrics.

After explaining the types of fibre-reinforced composites, it is important to understand that it exists a great variety of fibres. In this case, that will only be explained two types, which were the ones used in the project: carbon and glass fibres.

Carbon fibres are a high-performance material. In terms of specific properties, these fibres stand for (Callister and Rethwisch 2007):

1. Highest specific modulus and specific strength of all reinforcing fibre materials;
2. Retain their high tensile modulus and high strength at elevated temperatures;
3. At room temperature, carbon fibres are not affected by moisture or a wide variety of solvents, acids and bases;
4. Exhibit a diversity of physical and mechanical characteristics allowing composites incorporating these fibres to have specific engineered properties.

One classification scheme for carbon fibres is by tensile modulus; on this basis, the four classes are standard, intermediate, high, and ultra-high moduli. In this project, it is going to be used the standard one.

When talking about the glass fibres, they are popular as a fibre reinforcement material for some motives:

1. It is easily drawn into high-strength fibres from the molten state;
2. It is readily available and may be fabricated from a glass-reinforced plastic economically, using a wide variety of composite manufacturing techniques;
3. As a fibre, it is relatively strong, and when embedded in a matrix, it produces a composite having a very high specific strength
4. When coupled with the various plastics, it possesses a chemical inertness that renders the composite useful in a variety of corrosive environments

Getting the resultant laminate, it is important to know the elastic properties of the laminate. One of the primary factors which determine the properties of composites is the relative proportions of the fibres and matrix. The proportions can be in terms of weight or volume fractions. For theoretical analysis, volume fractions are better to obtain despite the weight fractions are easier to get during the construction process and experimentally (Shenoi and Wellicome 1993).

Considering a case with weights/volumes of fibres, matrix and net composite being w_f/v_f, w_m/v_m and w_c/f_c respectively. Letters f, m and c are used to indicate fibre, matrix and composite respectively. Volume and weight fractions are denoted by V and W respectively (Shenoi and Wellicome 1993). So, for volumes:

$$v_c = v_f + v_m \tag{1}$$

$$V_f = \frac{v_f}{v_c} \ , V_m = \frac{v_m}{v_c} \tag{2}$$

and for weights:

$$w_c = w_f + w_m \tag{3}$$

$$W_f = \frac{w_f}{w_c} \ , W_m = \frac{w_m}{w_c} \tag{4}$$

Knowing these relations, the density of the composite it is established by:

$$\rho_c v_c = \rho_f v_f + \rho_m v_m \tag{5}$$

Dividing both sides for v_f and using the definitions of volume fractions,

$$\rho_c = \rho_f V_f + \rho_m V_m \tag{6}$$

Using the weight terms:

$$\rho_c = \frac{1}{\left(\frac{W_f}{\rho_f}\right) + \left(\frac{W_m}{\rho_m}\right)} \tag{7}$$

At this point, it is important to explicit the FVF and FWF (Fibre weight fraction). Starting with the fibre volume fraction from the fibre weight fraction:

$$FVF = \frac{1}{\left[1 + \frac{\rho_f}{\rho_m} * \left(\frac{1}{FWF} - 1\right)\right]} \tag{8}$$

With some mathematical manipulation, it can obtain the fibre weight fraction from the fibre volume fraction (Gurit Holding AG 2000):

$$FWF = \frac{\rho_f * FVF}{\rho_m + [(\rho_f - \rho_m) * FVF]} \tag{9}$$

Like it can be easily observed, the two fractions depend one on each other, but the fibre weight fraction, as said before, can be calculated experimentally, knowing the mass of resin and matrix applied. So, the fibre weight fraction can be calculated as:

$$FWF = \frac{m_f}{m_f + m_m} \tag{10}$$

In terms of important definitions, there is one more that is going to be used in this project which is, the cured ply thickness (CPT). This expression will give the thickness, in millimeters of each ply, taking account the fibre area weight (W_F) in grammes per square meter, the fibre densities, expressed in grammes per cubic centimeter and the fibre volume fraction for each type of fibre. So, the expression is going to be:

$$t = \frac{W_F}{\rho_f * FVF * 1000} \ [mm] \tag{11}$$

3.1.1. Manufacturing Processes

In composites, the choice of manufacturing process depends on the type of matrix and fibres, the temperature required to form the part and to cure the matrix and the relation between cost and effectiveness of the process. Each process enforces limitations on the structural design. Processing the polymer matrix composites involves operations such as fibre placement along the required orientations; impregnation of the fibres with the resin; consolidation of the impregnated fibres to remove the excess resin, air and volatile substances; cure of the polymer; extraction from the mould and finishing operations, such as trimming (Barbero 2010).

In the fabrication of the fin, two mixing processes are used: hand lay-up and compression moulding. Starting with the hand lay-up technique, also called *wet lay-up* it involves manual placement of the dry reinforcements in the mould and the subsequent application of the resin like it can be observed in the Figure 3.4. The process can be divided into four basic moments: mould preparation, gel coating, lay-up and curing.

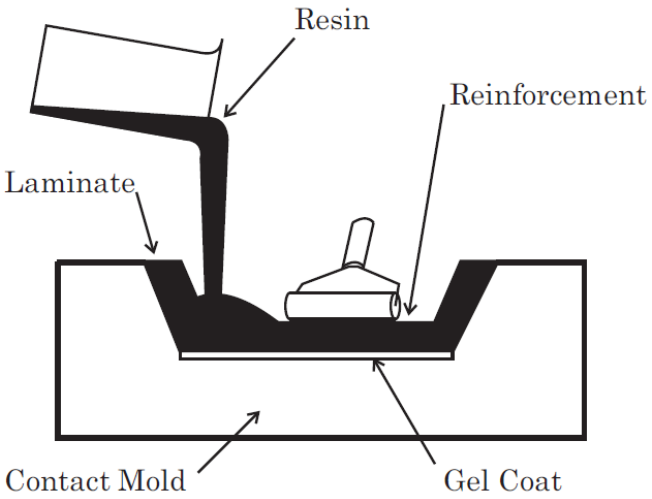

Figure 3.4- Hand Lay-up Process

The mould may be made of wood, plaster, plastics, composites, or metals depending on the number of parts, cure temperature, pressure, etc. In this case, because it is considered a permanent mould, that is used for long runs, the mould is made of aluminum. A gel coating is applied after the preparation of the mould to give a good final surface appearance. This resin lamina is applied to the mould before the reinforcements. This surface also forms a protective lamina through which the fibrous reinforcements do not penetrate and the product may require no subsequent finishing operations. In relation of the material preparations and fibre placement, some premeasured resins and catalysts are mixed together carefully to achieve the predefined and calculated values. The resin mixture is then applied to the fibres. Serrated hand rollers are used to compact the material against the mould to ensure whole air removal. After the complete impregnation of the resin with the fibres, the process used to finish the fin is the compression moulding. This process employs matched male and female metal dies to form the mould. The compound formed by the reinforcements and the resin used in the lay-up previous process is charged into the mould. A hydraulic press, using heat and a high pressure, is used to create the part from the fibres and resin by closing the male and female halves of the mould. The pressure is released and the part is ejected from the mould like it can be seen in Figure 3.5. Post moulding operations include the removal of flash and the post-curing process (Barbero 2010).

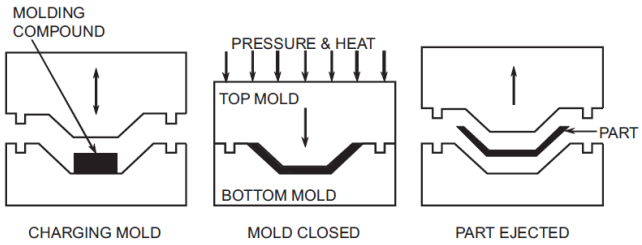

Figure 3.5- Compression Moulding

To be able to analyze the fin properly with all these properties and complex characteristics, finite element analysis was used.

3.2 Finite Element Analysis

Finite Element Analysis (FEA) is a numerical method for solving problems of engineering and mathematical physics. It is very useful for problems with complicated geometries, loadings and material properties, where the analytical solutions cannot be obtained easily. Finite Element Method has the objective to analyze with high accuracy, where it is necessary to understand the physical behavior of a complex object (strength, heat transfer capability, fluid flow, etc.). After the study, it should be possible to predict the performance and behavior, to calculate safety margin and to identify the weakness of the design. An optimal design should be achieved with an iterative project.

Considering an arbitrary 3D solid in Figure 3.6, with volume V and surface S, subjected to surface forces p_s per unit area and body forces p_v per unit volume.

$$p_s^t = [p_{sx} \quad p_{sy} \quad p_{sz}] \tag{12}$$

$$p_v^t = [p_{vx} \quad p_{vy} \quad p_{vz}] \tag{13}$$

Similarly, the displacements can be written as:

$$u^t = [u \quad v \quad w] \tag{14}$$

Internal stresses and strains can also be listed as column matrices in terms of the three components:

$$\sigma^t = [\sigma_{xx} \quad \sigma_{yy} \quad \sigma_{zz} \quad \sigma_{xy} \quad \sigma_{yz} \quad \sigma_{zx}] \tag{15}$$

$$\varepsilon^t = [\varepsilon_{xx} \quad \varepsilon_{yy} \quad \varepsilon_{zz} \quad \varepsilon_{xy} \quad \varepsilon_{yz} \quad \varepsilon_{zx} \tag{16}$$

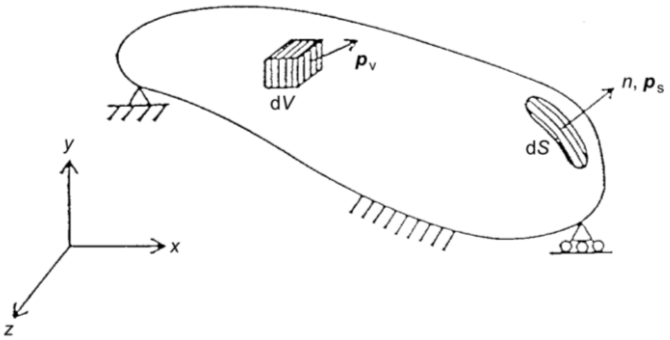

Figure 3.6- General Continuum (Matthews et al. 2000)

In this notation, σ_{xx} is a direct stress and σ_{xy} is a shear stress.

The external virtual work done is:

$$\begin{aligned} \int_S (p_{sx}u + p_{sy}v + p_{sz}\overline{w})dS + \int_V (p_{vx}u + p_{vy}v + p_{vz}\overline{w})dV \\ = \int_S p_s^t u \; dS + \int_V p_v^t u \; dV \end{aligned} \tag{17}$$

This can also be written in terms of stresses over the strains:

$$\int_V (\sigma_{xx}\varepsilon_{xx} + \sigma_{yy}\varepsilon_{yy} + \sigma_{zz}\varepsilon_{zz} + \sigma_{xy}\varepsilon_{xy} + \sigma_{yz}\varepsilon_{yz} + \sigma_{zx}\varepsilon_{zx})dV = \int_V \sigma^t\varepsilon \; dV \tag{18}$$

After this, it is important to equate the two expressions for work and enforce compatibility using the following general equations:

$$\varepsilon_{xx} = \frac{du}{dx}, \quad \varepsilon_{xy} = \frac{du}{dy} + \frac{dv}{dx}, etc \tag{19}$$

Then, and using the mathematical identity derived from Gauss's Theorem, the principal of virtual displacements becomes:

$$\int_V \sigma^t \partial u \; dV = \int_S u^t[\partial^t n]\sigma \; dS - \int_V u^t \partial^t \sigma \; dV \tag{20}$$

The principal of virtual displacements is being used as an integral, giving the ability to write complete volume and surface integrals as a summation of all the element integrals:

$$\sum_{elements} \int_{Vg} \sigma^t \varepsilon \, dV = \sum_{elements} \left[\int_{Sg} p_s u \, dS + \int_{Sg} p_v^t u \, dV \right] \tag{21}$$

where S_g and V_g represent the surface and volume of gth element.

Considering a flat plate with triangular mesh as represented in Figure 3.7, with a 2D stress field and a linear displacement field, it can be written that:

$$u = N_1 d_1 + N_2 d_3 + N_3 d_5 \tag{22}$$

Where shape functions N(x,y) are linear (in this specific case). Similarly, for the other displacement component:

$$v = N_1 d_2 + N_2 d_4 + N_3 d_6 \tag{23}$$

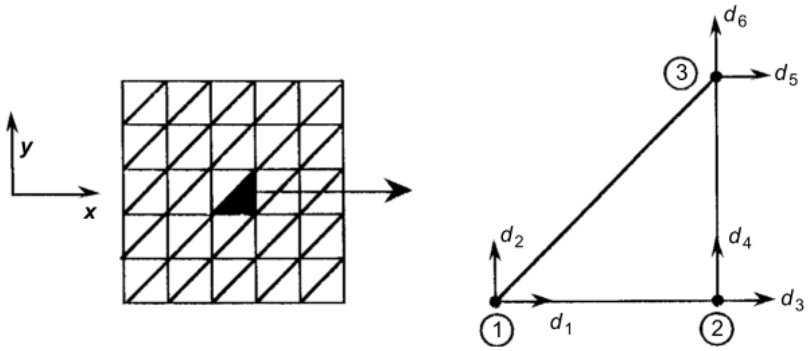

Figure 3.7- Triangular Element with Linear Shape Function (Matthews et al. 2000)

Going for the next stage and applying compatibility:

$$\varepsilon = \partial u = \partial N d_g = B d_g \tag{24}$$

Where the 6x6 for this specific example is an array of constants.

The internal work can now be specified as:

$$\int_{Vg} \sigma^t \varepsilon \, dV = \int_{Vg} \varepsilon^t E \, \varepsilon \, dV = \int_{Vg} d_g^t B^t E B \overline{d_g} \, dV \tag{25}$$

Considering the element work equal to $d_g^t k_g \overline{d_g}$, where:

$$k_g = \int_{V_g} B^t E B \; dV \tag{26}$$

Is known as the element stiffness matrix. After some manipulation, where

$$P_g = \int_{V_g} N^t \, p_v dV + \int_{S_g} N^t \, p_s dS \tag{27}$$

are the nodal forces, which are measures convenient to use. The total global list of displacements is:

$$r^t = [r_1 \;\; r_2 \;\; r_3 \;\; ... \;\; r_n] \tag{28}$$

Knowing that K is the structure's stiffness matrix and R is the global list of kinematically equivalent forces,

$$K = \sum \; k_g \qquad and \qquad R = \sum \; P_g \tag{29}$$

Assembling both K and R, the principle of virtual displacements as

$$r^t K - R^t \; r = 0 \tag{30}$$

$$Kr = R \tag{31}$$

Knowing r, particular values of d are selected for the element level and, understanding that ε=Bd_g and σ=Eε, this is the basis of the modern finite element method for stresses and strains. Equating local and global nodal displacements continuity of the structure's nodal displacements is assured (Matthews et al. 2000).

3.2.1. FEM in Composites

Although composite materials are now in extensive applications, their design is specially challenging because, unlike conventional materials, the composite material itself is design alongside with the composite structure. The preliminary design is grounded in the concept of a state of plane stress in laminate. Recent commercial finite element analysis software's, such as ANSYS, with pre and post-processing applications have made detailed analysis of composites easier to the designer but, still quite changeling (Barbero 2008b).

One of the main concerns is that, to correctly design and analyze a composite structure, software's requires a lot of input information, such as material properties, which are not quite easily available, making

the structural design with composite materials a much more demanding task. Other question is the complexity of interaction of the fibres and of the fibres with the matrix. These interactions are most of the problems after the preliminary design, since the software need to be aware of the possibilities of can such a complex structure fail.

3.3 Failure Criterion

Failure criteria for fibre reinforced plastic composites has been studied for over the last four decades. The number of approaches that have been proposed demonstrates that failure criteria is still today an important research topic. When talking about lamina failure criteria, it can be divided in two main groups: failure criteria associated with failure modes and failure criteria not associated with failure modes. In the first one, most of the criteria proposed identify some failure modes such as: fibre fracture, transverse matrix cracking and shear matrix cracking. Maximum Strain Criterion, Maximum Stress Criterion and Puck are some criteria that fits in this first category. In other way, some criteria are not coupled with a failure mode, only indicating if occurs failure or not. This second group includes all polynomial criteria, using mathematical expressions to describe the failure surface as a function of the material strengths. The most general polynomial criterion for composite materials is the one proposed by Tsai-Wu in 1971. This criterion takes in account some features as the lack of isotropy in composite laminates using appropriate constitutive equations (Camanho 2002). This last criterion was the one used in this project because it although does not specify the failure mode, it is known that includes most of the common failure modes in composite materials.

Tsai and Wu (1971) created a strength criterion for composites is that there exists a failure surface in the stress space in the following scalar form:

$$f\ \sigma_k\ = F_i\sigma_i + F_{ij}\sigma_i\sigma_j = 1 \tag{32}$$

where the indexes *i, j, k=1,..,6* are used in a 3D case (repeated indexes imply summation); and F_i and F_{ij} are second and fourth rank tensors, respectively. Expanding the Equation (32) gets this:

$$
\begin{aligned}
F_1\sigma_1 + F_2\sigma_2 + F_3\sigma_3 + F_4\sigma_4 + F_5\sigma_5 + F_6\sigma_6 + F_{11}\sigma_1^2 + 2F_{12}\sigma_1\sigma_2 + 2F_{13}\sigma_1\sigma_3 \\
+ 2F_{14}\sigma_1\sigma_4 + 2F_{15}\sigma_1\sigma_5 + 2F_{16}\sigma_1\sigma_6 + F_{22}\sigma_2^2 + 2F_{23}\sigma_2\sigma_3 \\
+ 2F_{24}\sigma_2\sigma_4 + 2F_{25}\sigma_2\sigma_5 + 2F_{26}\sigma_2\sigma_6 + F_{33}\sigma_3^2 + 2F_{34}\sigma_3\sigma_4 \\
+ 2F_{35}\sigma_3\sigma_5 + 2F_{36}\sigma_3\sigma_6 + F_{44}\sigma_4^2 + 2F_{45}\sigma_4\sigma_5 + 2F_{46}\sigma_4\sigma_6 + F_{55}\sigma_5^2 \\
+ 2F_{56}\sigma_5\sigma_6 + F_{66}\sigma_6^2 = 1
\end{aligned}
\tag{33}
$$

where the higher order terms $F_{ijk}\sigma_i\sigma_j\sigma_k$ were ignored, because it is not practical from the operational point of view and cubic terms would make the failure surface open-ended. In relation to the terms, the linear one σ_i considers internal stresses showing the difference between positive and negative stress-induced failures. The quadratic terms $\sigma_i\sigma_j$ are the ones who define the ellipsoid in the stress-space.

As reported by Tsai and Wu (1971), this strength criterion has several features (some of them will not be explicit because are not important for this thesis) that need to be explicated:

1. Since it is a scalar equation, it is automatically invariant, making the interactions between all stress components independent of the material properties
2. The number of multiaxial stresses and special dimensions is determined by selecting a proper range of indices among 1 to 6. Anisotropy and 3-D cases present no conceptual effort
3. Being invariant, the equations (32) and (33) are valid for all coordinate systems, when valid for one single coordinate system.
4. The magnitude of interaction terms is constrained by the following inequality:

$$
F_{ii}F_{jj} - F_{ij}^2 \geq 0 \tag{34}
$$

   4.1. Repeated indices are not summations for this equation, where F_{ii} is simply one of the diagonal terms
   4.2. To be physically meaningful, the diagonal terms must be positive
   4.3. Off-diagonal terms can be positive or negative but they are constrained by the inequality (34)
   4.4. Geometrically, the inequality assures that the failure surface will intercept each stress axis, making the shape of the surface an ellipsoidal
   4.5. The inequality also ensures that the failure surface is not open-ended like a hyperboloid

3.4 Plane Stress Case

In composites, most of the materials are treated as anisotropic. However, due to the symmetry properties of the strength tensors, it can be assumed that both strength tensors (F_i and F_{ij}) are symmetric. The number of independent components is 6 and 21 for F_i and F_{ij} respectively.

$$F_i = \begin{Bmatrix} F_1 \\ F_2 \\ F_3 \\ F_4 \\ F_5 \\ F_6 \end{Bmatrix} \tag{35}$$

$$F_{ij} = \begin{bmatrix} F_{11} & F_{12} & F_{13} & F_{14} & F_{15} & F_{16} \\ & F_{22} & F_{23} & F_{24} & F_{25} & F_{26} \\ & & F_{33} & F_{34} & F_{35} & F_{36} \\ & & & F_{44} & F_{45} & F_{46} \\ & & & & F_{55} & F_{56} \\ & & & & & F_{66} \end{bmatrix} \tag{36}$$

For orthotropic materials, F_4, F_5 and F_6 are expected to disappear. If we assume that the change of sign does not change the failure stress, the coupling between normal and shear strengths will also vanish. For essentially the same reason, the shear strengths for especially orthotropic are all uncoupled; F_{45}=F_{56}=F_{64}=0. With these conditions expressed above, the number of independent variables reduced to 3 and 9 respectively (Tsai and Wu 1971).

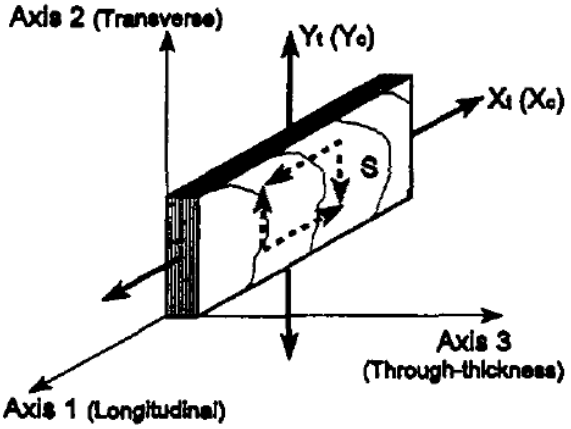

Figure 3.8- Plane Stress State (Clouston et al. 1998)

Now, the F_i and F_{ij} from (35) and (36), will be reduced to:

$$F_i = \begin{Bmatrix} F_1 \\ F_2 \\ F_6 \end{Bmatrix} \tag{37}$$

$$F_{ij} = \begin{bmatrix} F_{11} & F_{12} & F_{16} \\ & F_{22} & F_{26} \\ & & F_{66} \end{bmatrix} \tag{38}$$

For especially orthotropic materials:

$$F_6 = F_{16} = F_{26} = 0 \tag{39}$$

reducing F_i and F_{ij} to 2 and 4 independent components respectively. Equation (33) can be simplified into this:

$$F_1\sigma_1 + F_2\sigma_2 + F_{11}\sigma_1^2 + F_{22}\sigma_2^2 + 2F_{12}\sigma_1\sigma_2 + F_{66}\sigma_6^2 = 1 \tag{40}$$

considering Figure 3.8, the five principal strengths are tension and compression parallel to the direction of the fibre (X_t and X_c), tension and compression transverse to the direction of the fibre (Y_t and Y_c), and shear in the same plane (S). If we consider a uniaxial tension load in the direction 1, equation (40) becomes (Clouston et al. 1998):

$$F_1X_t + F_{11}X_t^2 = 1 \tag{41}$$

and for compression, failure becomes:

$$F_1X_c + F_{11}X_c^2 = 1 \tag{42}$$

solving them simultaneously and concerning compression strength as negative, the parameters F_1 and F_{11} can be solved as:

$$F_1 = \frac{1}{X_t} - \frac{1}{X_c} \tag{43}$$

$$F_{11} = \frac{1}{X_t X_c} \tag{44}$$

using similar manipulations, it can be shown that:

$$F_2 = \frac{1}{Y_t} - \frac{1}{Y_c} \tag{45}$$

$$F_{22} = \frac{1}{Y_t Y_c} \tag{46}$$

$$F_{66} = \frac{1}{S^2} \tag{47}$$

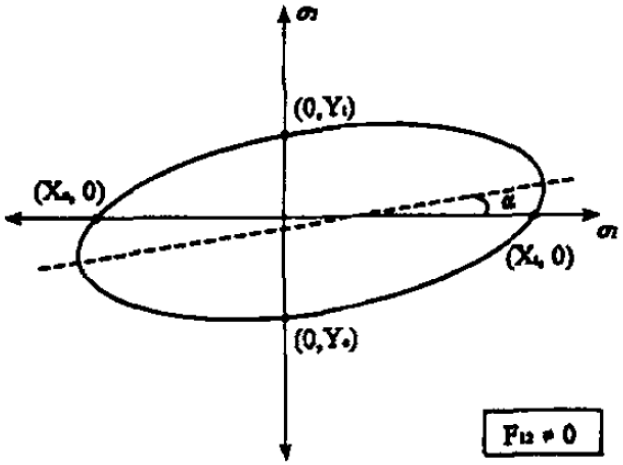

Figure 3.9- Sample Tsai-Wu Failure Surface (Clouston et al. 1998)

The surface forms an ellipsoid in stress space, where F_{12} characterizes the rotation (α) of the ellipsoid with respect to the stress coordinate axis. Difficulties have been encountered when evaluating F_{12} experimentally due to its sensitivity to experimental variation (Clouston et al. 1998). Narayanaswami and Adelman (1977) described that assigning F_{12} to zero was acceptable for filamentary composites.

3.5 Stress-Strain Relations

The increasing use of advanced composites for structural application has represented the main motivation to develop refined theories for single-layer or multilayered orthotropic beams, where the limits of classical theories are removed. It is well known that the classical Saint-Venant warping is exact only for beams with unrestrained ends and tip loads (Savoia and Tullini 1996).

Starting with the material's constants, the most general form of Hooke's Law for a linear elastic material is:

$$\begin{bmatrix} \sigma_1 = \sigma_{xx} \\ \sigma_2 = \sigma_{yy} \\ \sigma_3 = \sigma_{zz} \\ \sigma_4 = \sigma_{yz} \\ \sigma_5 = \sigma_{xz} \\ \sigma_6 = \sigma_{xy} \end{bmatrix} = \begin{bmatrix} C_{11} & C_{12} & C_{13} & C_{14} & C_{15} & C_{16} \\ C_{21} & C_{22} & C_{23} & C_{24} & C_{25} & C_{26} \\ C_{31} & C_{32} & C_{33} & C_{34} & C_{35} & C_{36} \\ C_{41} & C_{42} & C_{43} & C_{44} & C_{45} & C_{46} \\ C_{51} & C_{52} & C_{53} & C_{54} & C_{55} & C_{56} \\ C_{61} & C_{62} & C_{63} & C_{64} & C_{65} & C_{66} \end{bmatrix} \begin{bmatrix} \varepsilon_1 = \varepsilon_{xx} \\ \varepsilon_2 = \varepsilon_{yy} \\ \varepsilon_3 = \varepsilon_{zz} \\ \varepsilon_4 = \varepsilon_{yz} \\ \varepsilon_5 = \varepsilon_{xz} \\ \varepsilon_6 = \varepsilon_{xy} \end{bmatrix} \tag{48}$$

where each stress component depends on all strain components. The 36 C_{ij}'s are material constants called the stiffness. The matrix of stiffness is called the stiffness matrix. These equations imply that a normal stress σ_{xx} will induce an element to not only stretch in x direction and contract laterally but to undergo shear strain to, as shown in the Figure 3.10.

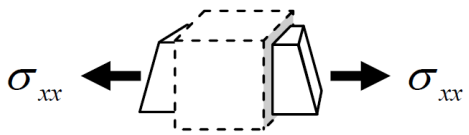

Figure 3.10- Element undergoing shear strain when subjected to normal stress only (Kelly 2015)

The equations from (48) can be updated so that the strains are given explicitly in terms of stresses:

$$\begin{bmatrix} \varepsilon_1 \\ \varepsilon_2 \\ \varepsilon_3 \\ \varepsilon_4 \\ \varepsilon_5 \\ \varepsilon_6 \end{bmatrix} = \begin{bmatrix} S_{11} & S_{12} & S_{13} & S_{14} & S_{15} & S_{16} \\ & S_{22} & S_{23} & S_{24} & S_{25} & S_{26} \\ & & S_{33} & S_{34} & S_{35} & S_{36} \\ & & & S_{44} & S_{45} & S_{46} \\ & & & & S_{55} & S_{56} \\ & & & & & S_{66} \end{bmatrix} \begin{bmatrix} \sigma_1 \\ \sigma_2 \\ \sigma_3 \\ \sigma_4 \\ \sigma_5 \\ \sigma_6 \end{bmatrix} \tag{49}$$

where the S_{ij}'s are called compliances and the matrix S is called the compliance matrix. The bottom half has been omitted because is symmetric. Although it is difficult to model full anisotropic materials,

fortunately, many materials which are not fully isotropic, still have some material symmetries which simplify the equations above. In this case, it will be discussed the orthotropic linear elasticity.

An orthotropic material is one which has three orthogonal planes of microstructural symmetry. Three mutual perpendicular planes of symmetry can be passed through each point in a continuum model. The x, y and z axes are called material directions.

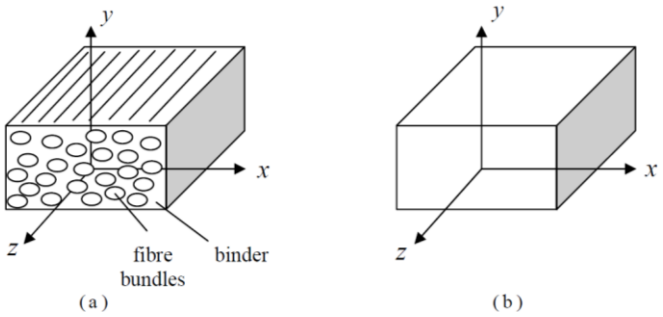

Figure 3.11- Orthotropic Material; (a) Microstructural Detail; (b) Continuum Model (Kelly 2015)

From equations (48), the stresses induced by a shear strain (ε_6) are:

$$\begin{aligned} \sigma_1 &= C_{16}\varepsilon_6 \ , \qquad \sigma_2 = C_{26}\varepsilon_6 \ , \qquad \sigma_3 = C_{36}\varepsilon_6 \\ \sigma_4 &= C_{46}\varepsilon_6 \ , \qquad \sigma_5 = C_{56}\varepsilon_6 \ , \qquad \sigma_6 = C_{66}\varepsilon_6 \end{aligned} \tag{50}$$

Due to the symmetry, orthotropic materials are subjected to shear strain ε_6 and $-\varepsilon_6$, as it is the Figure 3.12.

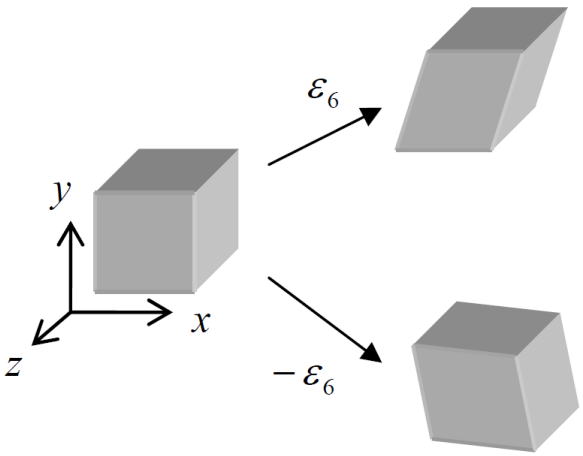

Figure 3.12- Orthotropic Material Undergoing Shear Strains (Kelly 2015)

the induced stresses by shear are also:

$$\begin{aligned} \sigma'_1 &= -C_{16}\varepsilon_6 \ , \qquad \sigma'_2 = -C_{26}\varepsilon_6 \ , \qquad \sigma'_3 = -C_{36}\varepsilon_6 \\ \sigma'_4 &= -C_{46}\varepsilon_6 \ , \qquad \sigma'_5 = -C_{56}\varepsilon_6 \ , \qquad \sigma'_6 = -C_{66}\varepsilon_6 \end{aligned} \tag{51}$$

Due to the symmetry of the material, it is expected to have the normal stresses to be the same, but the shear ones to have opposite sign. This implies that:

$$C_{16} = C_{26} = C_{36} = C_{46} = C_{56} = 0 \tag{52}$$

Similar conclusions can be obtained in the other two planes for respective shear strains:

$$\begin{aligned} &\varepsilon_5\text{: } C_{15} = C_{25} = C_{35} = C_{45} = 0 \\ &\varepsilon_4\text{: } C_{14} = C_{24} = C_{34} = 0 \end{aligned} \tag{53}$$

Reducing the stiffness matrix and obtaining only nine independent elastics constants:

$$\begin{bmatrix} \sigma_1 \\ \sigma_2 \\ \sigma_3 \\ \sigma_4 \\ \sigma_5 \\ \sigma_6 \end{bmatrix} = \begin{bmatrix} C_{11} & C_{12} & C_{13} & 0 & 0 & 0 \\ & C_{22} & C_{23} & 0 & 0 & 0 \\ & & 0 & 0 & 0 & 0 \\ & & & 0 & 0 & 0 \\ & & & & 0 & 0 \\ & & & & & \end{bmatrix} \begin{bmatrix} \varepsilon_1 \\ \varepsilon_2 \\ \varepsilon_3 \\ \varepsilon_4 \\ \varepsilon_5 \\ \varepsilon_6 \end{bmatrix} \tag{54}$$

Inverting the algebraic formulation in (54) and introducing elastic constants E, ν and G, in gives:

$$\begin{bmatrix} \varepsilon_1 \\ \varepsilon_2 \\ \varepsilon_3 \\ \varepsilon_4 \\ \varepsilon_5 \\ \varepsilon_6 \end{bmatrix} = \begin{bmatrix} \frac{1}{E_1} & -\frac{\nu_{21}}{E_2} & -\frac{\nu_{31}}{E_3} & & & \\ -\frac{\nu_{12}}{E_1} & \frac{1}{E_2} & -\frac{\nu_{32}}{E_3} & & & \\ -\frac{\nu_{13}}{E_1} & -\frac{\nu_{23}}{E_2} & \frac{1}{E_3} & & & \\ & & & \frac{1}{2G_{23}} & & \\ & & & & \frac{1}{2G_{13}} & \\ & & & & & \frac{1}{2G_{12}} \end{bmatrix} \begin{bmatrix} \sigma_1 \\ \sigma_2 \\ \sigma_3 \\ \sigma_4 \\ \sigma_5 \\ \sigma_6 \end{bmatrix} \tag{55}$$

where E_i is the Young Modulus (stiffness) of the material in the direction *i=1,2,3*; ν_{ij} is the Poisson ratio representing the ratio of a transverse strain to the applied in uniaxial tension; G_{ij} are the shear moduli representing the shear stiffness in the corresponding plane. From the symmetry of the matrix:

$$\nu_{23}E_3 = \nu_{32}E_2, \quad \nu_{13}E_3 = \nu_{31}E_1, \quad \nu_{12}E_2 = \nu_{21}E_1 \tag{56}$$

The orthotropic materials are considered to have no shear coupling. So, normal stresses result only in normal strains and shear stresses result only in shear strains, neglecting the effects represented in Figure 3.10.

4 Analyzing the Model

4.1 Global Model

To understand the real importance of the fin, it is necessary to comprehend the global model of the windsurfer diagram of forces. The overall problem is shown in Figure 4.1. The problem could be more specified but, for the strength analysis of the fin, this diagram is enough for the objective of the study. So, as it can be observed, the fin lift is very important to balance with the sail side-force, applied in a much bigger area than the fin's area, so it needs to have high strength values to hold on.

Relating the fin with the board, the fin is attached to a tuttle box, which will be fixed to the board. In the numerical analysis, it will only be considered the fin itself, assuming fixed support like it was the box. Relations between strains and stresses are explained in the chapter Theoretical Background. Due to fact that two dimensions are much bigger than one of them (thickness very small compared with the span and cord), the theory bellow this is much closer to a cantilever plate than a fixed support beam. Despite this, none of these two classical approaches will be completely correct because we are dealing with composites and it there is a lot of non-linearities that are not counted there.

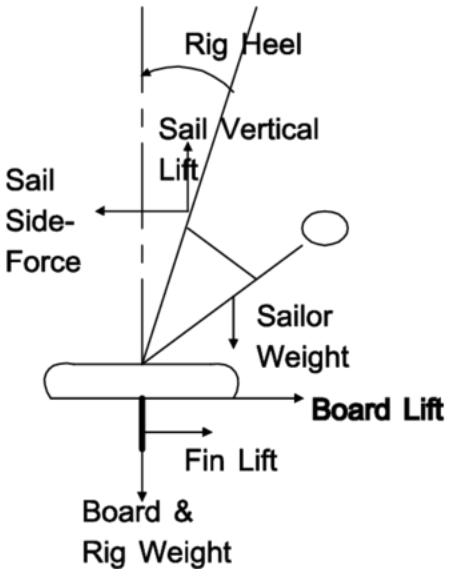

Figure 4.1- Global Force Diagram (Sutherland 1993)

4.2 37 RS-3 Standard Slalom Fin

The fin analyzed in the project is manufactured by the company F-Hot. The design of the fin was completely defined, not only exteriorly, but also in the disposition of the plies. In Figure 4.2, it can be seen the complete fin, with the tuttle box which is going to be fixed to the board.

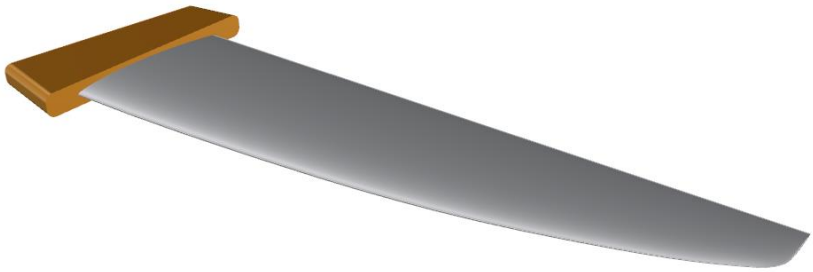

Figure 4.2- Fin 37 RS-3 Standard Slalom Fin with Tuttle Box

Although Figure 4.3 displays the complete setup of the fin, the part that is going to be analyzed is only the fin itself, so the box will not be part of any analysis. Taking out the box will make the analysis simpler and will be replaced by a fixed support boundary condition. Starting with the exterior design of the fin, the two major dimensions of the fin (span and chord) are defined in the figure below, in millimeters.

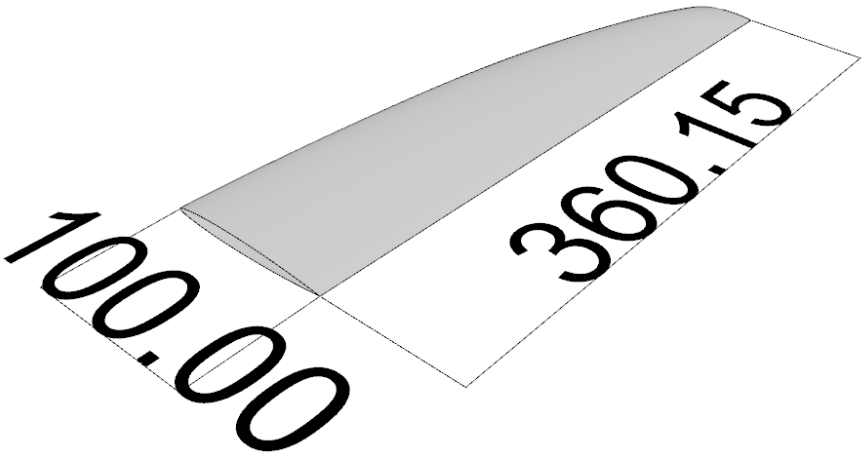

Figure 4.3- Dimensions of the Fin (Span and Chord) in millimeters

This fin is made for slalom, so, as explained in the chapter 2 State of the Art, fins for this type of windsurf activity are set to have good strength due to the sudden changes of the direction. The company F-Hot sent the geometry of the fin in an *igs* file. This was only the external layout of the fin, which was

not the purpose of any change or even, an object of study to propose any other alternatives (in terms of shape).

After this, the internal arrangement of the laminate should be arranged, replicating the plies that were in the real-scale model. To do this, F-Hot sent a sketch of the arrangement of the plies, specifying where the plies were supposed to be, the type (unidirectional or woven) and the type of the fibre (carbon or E-glass fibres). This sketch can be observed in Figure 4.10.

Using the equations from (5) to (11), and using the FWF (fibre weight fraction) that F-Hot provided, it was important to first define the densities of the fibres and the matrix. For this, the density of the woven carbon fibre was taking from ANSYS, the unidirectional carbon fibre was from Paul Miller, the unidirectional E-glass was from Exel (2016) and the density of the matrix (epoxy resin) was from Gurit Holding AG (2000).

$$\rho_m = 1.2\ g/cm^3 \tag{57}$$

$$\rho_{e-glass} = 2.580\ g/cm^3 \tag{58}$$

$$\rho_{carbon-UD} = 1.5003\ g/cm^3. \tag{59}$$

$$\rho_{carbon-woven} = 1.47\ g/cm^3 \tag{60}$$

F-Hot used 97 grams of reinforcements (summing all the reinforcements used to produce one fin) and 140 grams of epoxy resin (matrix). In this way:

$$FWF = \frac{m_f}{m_f + m_m} = 40.92\ \% \approx 41\% \tag{61}$$

and using equation (8):

$$FVF_{carbon\_UD} = 39.56\% \tag{62}$$

$$FVF_{carbon\_woven} = 40.04\% \tag{63}$$

$$FVF_{E-glass} = 27.57\% \tag{64}$$

These values gave the ability to calculate the thickness of a ply of each type of reinforcement, using the equation (11). This is only numerical because it is impossible to ensure that the plies have such precise values. For the woven carbon plies, there is two different options in terms of weight per area: the 100g/m^2 and the 200g/m^2, and naturally the second one will have the double of the thickness of the first.

$$t_{carbon-woven\ (100g/m^2)} = 0.170\ mm \tag{65}$$

$$t_{carbon-woven\ (200g/m^2)} = 0.374\ mm \tag{66}$$

$$t_{carbon-UD} = 0.169\ mm \tag{67}$$

$$t_{e-glass} = 0.281\ mm \tag{68}$$

In the Table 4-1, Table 4-2, Table 4-3, Table 4-4 and Table 4-5, are demonstrated the final values for the input to use in ANSYS ACP pre-processor.

Table 4-1- Input Values Carbon Woven 100g/m²

Carbon Woven- 100g/m²			
Density	ρ	g/cm^3	**1.470**
Orthotropic Elasticity	E_x	Pa	**6.13E+10**
	E_y	Pa	**6.13E+10**
	E_z	Pa	**6.9E+09**
	ν_{xy}	--	**0.04**
	ν_{yz}	--	**0.3**
	ν_{xz}	--	**0.3**
	G_{xy}	Pa	**1.95E+10**
	G_{yz}	Pa	**2.7E+09**
	G_{xz}	Pa	**2.7E+09**
Orthotropic Stress Limits	$\sigma_{x\ (T)}$	Pa	**8.05E+08**
	$\sigma_{y\ (T)}$	Pa	**8.05E+08**
	$\sigma_{z\ (T)}$	Pa	**5.00E+07**
	$\sigma_{x\ (C)}$	Pa	**-5.1E+08**
	$\sigma_{y\ (C)}$	Pa	**-5.1E+08**
	$\sigma_{z\ (C)}$	Pa	**-1.7E+08**
	τ_{xy}	Pa	**1.25E+08**
	τ_{yz}	Pa	**6.50E+07**
	τ_{xz}	Pa	**6.50E+07**
Orthotropic Strain Limits	$\varepsilon_{x\ (T)}$	--	**0.0126**
	$\varepsilon_{y\ (T)}$	--	**0.0126**
	$\varepsilon_{z\ (T)}$	--	**0.008**
	$\varepsilon_{x\ (C)}$	--	**-0.0102**
	$\varepsilon_{y\ (C)}$	--	**-0.0102**
	$\varepsilon_{z\ (C)}$	--	**0.012**
	ε_{xy}	--	**0.22**
	ε_{yz}	--	**0.019**
	ε_{xz}	--	**0.019**

Table 4-2- Input Values Carbon Woven 200g/m²

Carbon Woven- 200g/m²			
Density	ρ	g/cm³	**1.470**
Orthotropic Elasticity	E_x	Pa	**3.07E+10**
	E_y	Pa	**3.07E+10**
	E_z	Pa	**3.45E+09**
	ν_{xy}	--	**0.04**
	ν_{yz}	--	**0.3**
	ν_{xz}	--	**0.3**
	G_{xy}	Pa	**1.95E+10**
	G_{yz}	Pa	**2.7E+09**
	G_{xz}	Pa	**2.7E+09**
Orthotropic Stress Limits	$\sigma_{x\ (T)}$	Pa	**8.05E+08**
	$\sigma_{y\ (T)}$	Pa	**8.05E+08**
	$\sigma_{z\ (T)}$	Pa	**5.00E+07**
	$\sigma_{x\ (C)}$	Pa	**-5.1E+08**
	$\sigma_{y\ (C)}$	Pa	**-5.1E+08**
	$\sigma_{z\ (C)}$	Pa	**-1.7E+08**
	τ_{xy}	Pa	**1.25E+08**
	τ_{yz}	Pa	**6.50E+07**
	τ_{xz}	Pa	**6.50E+07**
Orthotropic Strain Limits	$\varepsilon_{x\ (T)}$	--	**0.0126**
	$\varepsilon_{y\ (T)}$	--	**0.0126**
	$\varepsilon_{z\ (T)}$	--	**0.008**
	$\varepsilon_{x\ (C)}$	--	**-0.0102**
	$\varepsilon_{y\ (C)}$	--	**-0.0102**
	$\varepsilon_{z\ (C)}$	--	**0.012**
	ε_{xy}	--	**0.22**
	ε_{yz}	--	**0.019**
	ε_{xz}	--	**0.019**

Table 4-3- Input Values for Carbon UD

Carbon UD			
Density	ρ	g/cm^3	**1.500**
Orthotropic Elasticity	E_x	Pa	**5.861E+10**
	E_y	Pa	**2.413E+09**
	E_z	Pa	**2.413E+09**
	ν_{xy}	--	**0.3**
	ν_{yz}	--	**0.4**
	ν_{xz}	--	**0.3**
	G_{xy}	Pa	**6.89E+09**
	G_{yz}	Pa	**5.3E+09**
	G_{xz}	Pa	**6.89E+09**
Orthotropic Stress Limits	$\sigma_{x\ (T)}$	Pa	**1.38E+09**
	$\sigma_{y\ (T)}$	Pa	**6.07E+07**
	$\sigma_{z\ (T)}$	Pa	**6.07E+07**
	$\sigma_{x\ (C)}$	Pa	**-6.2E+08**
	$\sigma_{y\ (C)}$	Pa	**-5.2E+07**
	$\sigma_{z\ (C)}$	Pa	**-5.2E+07**
	τ_{xy}	Pa	**7.65E+07**
	τ_{yz}	Pa	**4.42E+07**
	τ_{xz}	Pa	**7.65E+07**
Orthotropic Strain Limits	$\varepsilon_{x\ (T)}$	--	**0.011454**
	$\varepsilon_{y\ (T)}$	--	**0.004013**
	$\varepsilon_{z\ (T)}$	--	**0.004013**
	$\varepsilon_{x\ (C)}$	--	**-0.00503**
	$\varepsilon_{y\ (C)}$	--	**-0.00484**
	$\varepsilon_{z\ (C)}$	--	**-0.00484**
	ε_{xy}	--	**0.00555**
	ε_{yz}	--	**0.004163**
	ε_{xz}	--	**0.00555**

Table 4-4- Input values for E-glass

E-Glass			
Density	ρ	g/cm^3	**2.580**
Orthotropic Elasticity	E_x	Pa	**1.2E+10**
	E_y	Pa	**2.67E+9**
	E_z	Pa	**2.67E+9**
	ν_{xy}	--	**0.3**
	ν_{yz}	--	**0.4**
	ν_{xz}	--	**0.3**
	G_{xy}	Pa	**5E+09**
	G_{yz}	Pa	**3.85E+09**
	G_{xz}	Pa	**5E+09**
Orthotropic Stress Limits	$\sigma_{x\ (T)}$	Pa	**1.1E+09**
	$\sigma_{y\ (T)}$	Pa	**3.50E+07**
	$\sigma_{z\ (T)}$	Pa	**3.50E+07**
	$\sigma_{x\ (C)}$	Pa	**-6.8E+08**
	$\sigma_{y\ (C)}$	Pa	**-1.2E+08**
	$\sigma_{z\ (C)}$	Pa	**-1.2E+08**
	τ_{xy}	Pa	**8.00E+07**
	τ_{yz}	Pa	**4.62E+07**
	τ_{xz}	Pa	**8.00E+07**
Orthotropic Strain Limits	$\varepsilon_{x\ (T)}$	--	**0.0244**
	$\varepsilon_{y\ (T)}$	--	**0.0035**
	$\varepsilon_{z\ (T)}$	--	**0.0035**
	$\varepsilon_{x\ (C)}$	--	**-0.015**
	$\varepsilon_{y\ (C)}$	--	**-0.012**
	$\varepsilon_{z\ (C)}$	--	**-0.012**
	ε_{xy}	--	**0.016**
	ε_{yz}	--	**0.012**
	ε_{xz}	--	**0.016**

For the epoxy resin, the input values are different. The values used were:

Table 4-5- Input Values for Epoxy Resin

Isotropic Elasticity	**E**	**MPa**	**9000**
	ν	--	0.37
	B (bulk)	MPa	5.27E+03
	G	MPa	1500
Tensile Yield Strength	σ	MPa	82

It is necessary to explain the type of materials used in the fin. It was explained in chapter 3.1 Composite Materials that were three types of materials that should be set: carbon fibre, E-glass fibres and epoxy resin. For these materials, software ANSYS asked for 27 specific values. These values were orthotropic elasticity values (E_x, E_y, E_z, ν_{xy}, ν_{yz}, ν_{xz}, G_{xy}, G_{yz} and G_{xz}) orthotropic stress limits ($\sigma_{x\,(T)}$, $\sigma_{y\,(T)}$, $\sigma_{z\,(T)}$, $\sigma_{x\,(C)}$, $\sigma_{y\,(C)}$, $\sigma_{z\,(C)}$, τ_{xy}, τ_{yz} and τ_{xz}) and orthotropic strain limits ($\varepsilon_{x\,(T)}$ $\varepsilon_{y\,(T)}$ $\varepsilon_{z\,(T)}$ $\varepsilon_{x\,(C)}$ $\varepsilon_{y\,(C)}$ $\varepsilon_{z\,(C)}$ ε_{xy}, ε_{yz} and ε_{xz}). To obtain all these values was the first task to do. For the woven carbon and the E-glass, the values from the materials of the ANSYS library were used, comparing them with other catalogues and, finally validated. For the epoxy resin, Miller (1991) was the preliminary source of information. Although these are pre-established values, those were quite different from the real fin, and some adjustments needed to be made, as is going to be explained in the chapter 5.2 Experimental Tests and Results. These adjustments were only for the values of the Young Moduli.

The finite element mesh is used to subdivide the CAD model into smaller domains called *elements*, over which a set of equations are solved. These equations approximately represent the governing equation of interest via a set of polynomial functions defined over each element. As these elements are made smaller and smaller, as the mesh is refined, the computed solution will approach the true solution. Despite this approach to a better solution, with a very refined mesh, the computational time will increase and it is very important to find a good balance between the acceptance of the solution and the time to achieve it. The mesh refinement was made in two major areas for two different reasons. First, near the root (fixed boundary condition) since it would be here that would appear higher values of stress and, consequently, important area to apply failure criteria. Second, near the leading edge, not because of higher values of stress but due to the necessity of the mesh to follow up the geometry of the fin. In this way, the mesh obtained and used was the one observed in Figure 4.4. For statistic, this mesh has 2597 nodes and 2610 elements, where most

of them are quadrilaterals but to give a better adaptively mesh to the curvature of the model, where the sizes of the faces go from 2 to 10 millimeters, giving the program the options the vary between these values.

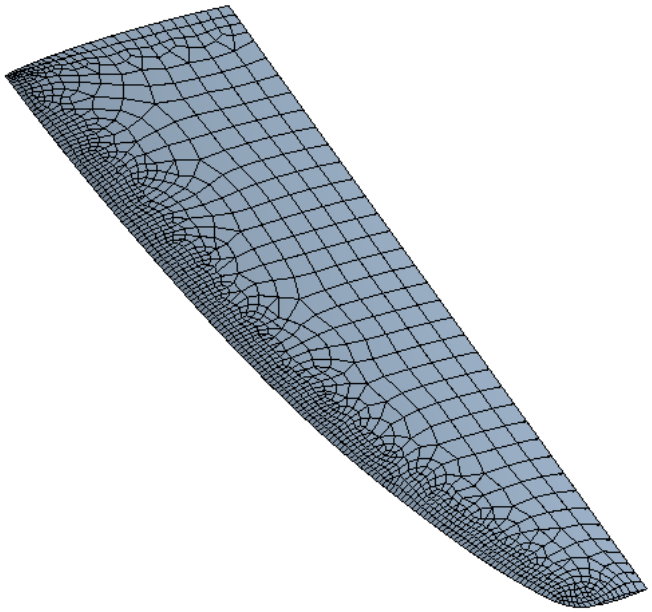

Figure 4.4- ANSYS Mesh

One of the points to balance the refinement of the mesh is the computational effort required to obtain the results. Higher refinement will lead to higher accuracy but will also bring higher numerical complexity and therefore, higher computational time. The mesh presented in Figure 4.4 was the final one, bringing accurate values. Knowing this, two refinements were made to the final mesh that was used, and can be seen in Figure 4.5 and Figure 4.6, and be analyzed with the respective computational time in Table 4-6.

Figure 4.5- Refinement 1

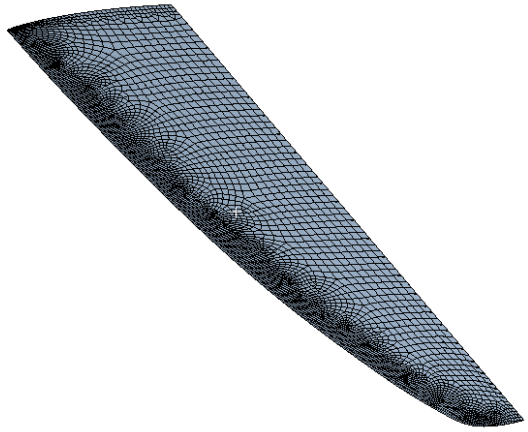

Figure 4.6- Refinement 2

Table 4-6- Mesh Refinement vs Computational Time

	Nodes	Elements	Computational Time
Final Mesh	2597	2610	11min 12 s
Refinement 1	4339	4308	30min 55s
Refinement 2	10079	10091	1h 39min

Analyzing Table 4-6, and considering that the results obtained with the "Final Mesh" were accurate, the increase of the computational time on each simulation is too much too considerate the usage of "Refinement 1" or even "Refinement 2", where the time needed does not bring considerable advantages that justify this growth in each simulation.

In the finite element analysis, it is necessary to define the type of the element that is going to be used. In this way, and knowing that the elements should be 3-D and should be able to present the deformations in all the directions, it was used the default element of ANSYS Workbench for shell elements, which is the SHELL181. This element is a four-node element with six degrees of freedom at each node: translations in the x, y, and z directions, and rotations about the x, y, and z axes. It is well-suited for linear, large rotation/deformation and large strain nonlinear applications.

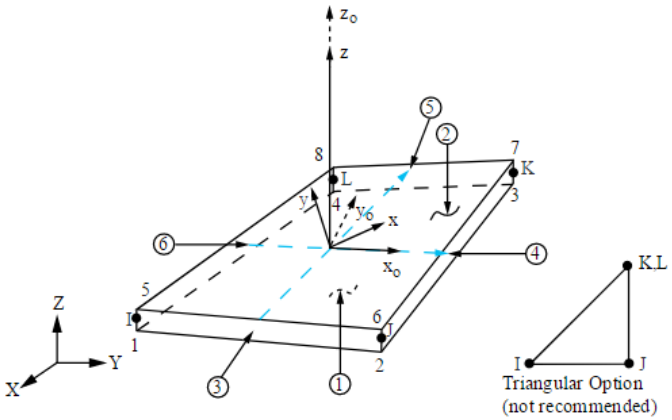

Figure 4.7- SHELL181 Finite Strain Shell Geometry (Ansys Inc. n.d.)

The element is defined by four nodes: I, J, K, and L. Element formulation is based on logarithmic strain and true stress measures. Element kinematics allow for finite membrane strains (stretching). However, the curvature changes within an increment are assumed to be small (Ansys Inc. n.d.).

After defining the mesh, the ACP pre-processor of ANSYS was used, which is a specific part of the software for composites and to make the plies. This ACP processor has two main parts: the pre-processor and post-processor. The first one is mainly used to define the composite fabrics, define the element orientation (to properly orient materials), define the ply sequence for groups of elements. The second one is to analyze the results, having the ability to apply failure criteria specific for composite.

Only five plies (from each side of the fin) are at full size, so it is necessary to define rules (boundaries) to set where the plies start and finish. After this, it is made a solid model, where the resin epoxy is selected to full fill the fin. In this way, the Figure 4.9 shows, from the top view, the thickness variation along the fin. As it can be observed, the region near the fixed support is going to be more filled with plies, due to the higher stresses when the model is subjected to a local vertical force. Back again to the cantilever, applying an intermediate load, these higher stresses are explained due the following figures and the consequent equations:

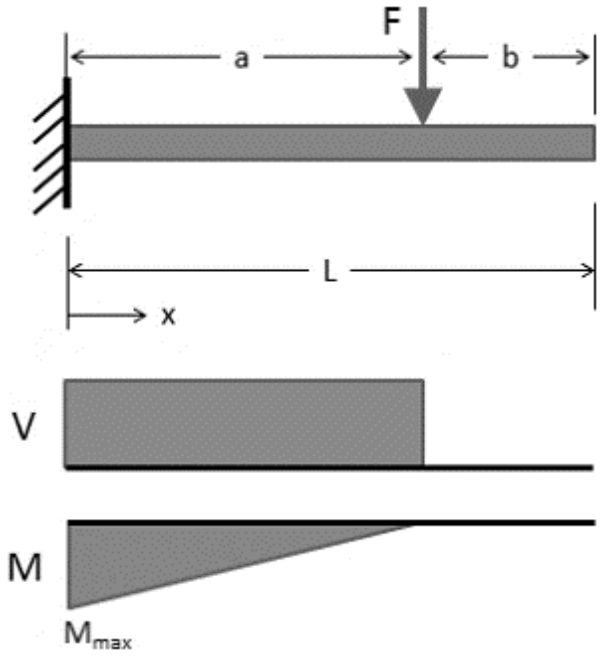

Figure 4.8- Cantilever, Intermediate Load

The graphics of shear and moment explicated in Figure 4.8, can be settled with the following equations. Starting with the value of the shear force produced by the remote force F:

$$V = +F \quad (0 \leq x \leq a) \tag{69}$$

$$V = 0 \quad (a \leq x \leq L) \tag{70}$$

Moving to the distribution of the moment:

$$M = -F(a - x) \quad (0 \leq x \leq a) \tag{71}$$

$$M = 0 \quad (a \leq x \leq L) \tag{72}$$

Analyzing first the distribution of shear forces, the value is equal to the force, from 0 to a, being zero from a until the tip. When going to the distribution of moment, the Equation (71) reveals that, from 0 to a, the value of the bending moment produced by the remote force, is maximum at the fixed support (x=0) and will decrease linearly until x=a. The value of the stress is directly related with the moment by the Equation (73).

$$\sigma_B = \frac{My}{I} \tag{73}$$

where σ_B is the stress induced by the bending moment M; y is the vertical distance away from the neutral axis and I is the moment of inertia around the neutral axis.

With this information and knowing that the composite fin does not behave like a cantilever (it has more non-linearities than are here considered), the understanding that the moment produced by a remote force is maximum at the fixed support, it is expected that the numerical values proves this theoretical demonstration.

Figure 4.9 illustrate that there is a higher thickness region until half of the span. This has the objective to make the fin capable to resist higher stresses near the fixed support when submitted to forces and start to bend. The real fin does not have such abrupt changes in the plies as we can see there, but the discretization into elements leads to this kind of approximations which will not have much influence in the results.

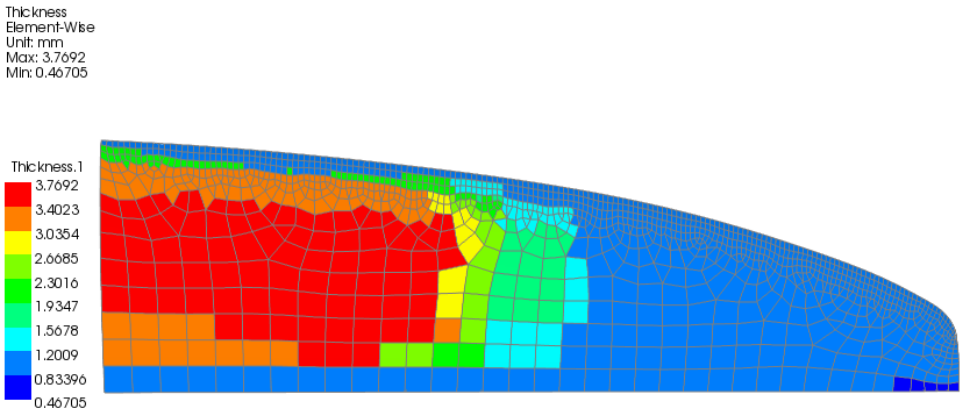

Figure 4.9- ACP Model Thickness

The disposition of the elements in mesh influences directly the disposition of the plies, because the elements are only full or empty, giving no option to have a part of the element with a ply and the rest with none. It is very important to understand the laminate of the fin, what plies are in there, what area do they occupy and what is the orientation of them. To comprehend this, the Figure 4.10 traduces how is organized. This knowledge will lead to a better comprehension of the results. In terms of representation, the figure only indicates half of the fin and the number of layers is organized from the outside to the inside. Both parts (named as *TOP* and *DOWN* for better organization during the project) are equal. In terms of tests, the TOP part will be under tension and the *DOWN* will be under compression. In further chapters,

are going to be called plies as, for example, *4.DOWN*. this refers to the 4^{th} ply counting from the surface under compression.

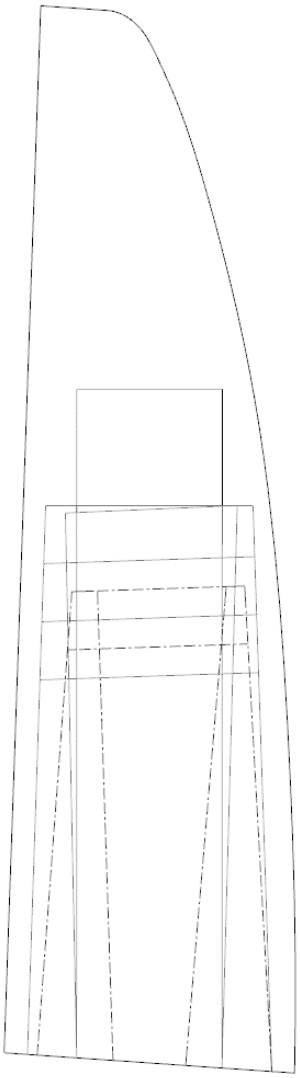

Figure 4.10- Layers Sketch

The layup of the fin included woven carbon and unidirectional carbon and glass reinforcements, but the exact layup schedule cannot be detailed here due to commercial considerations.

After creating the fin, selecting the elements and all the properties, the boundary conditions in the FE Model were set (that it is going to be replicated in the set-up of the experimental test) to give the best approximation to the fin in relation to the box where the fin is fixed. The boundary condition was set as shown in Figure 4.11.

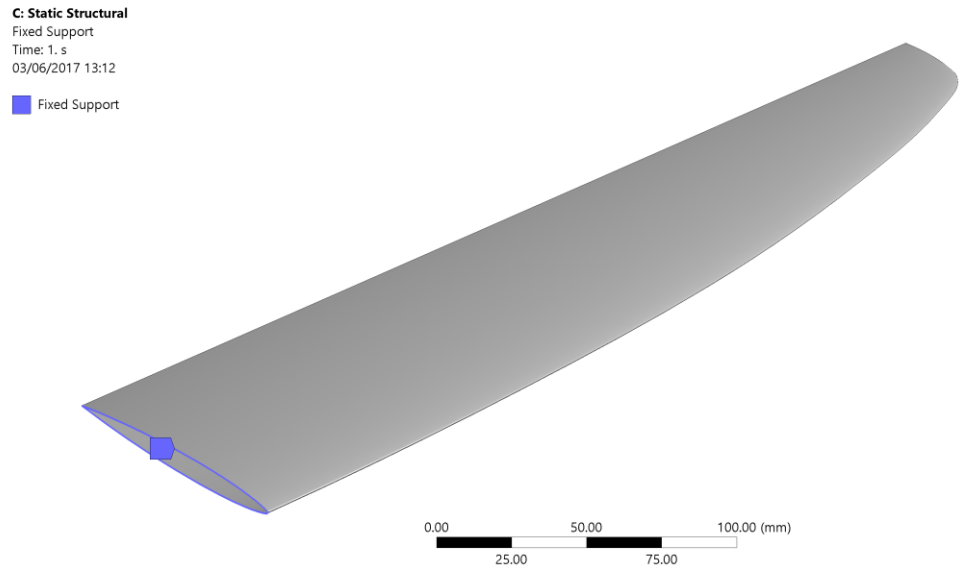

Figure 4.11- Boundary Conditions ANSYS

Only the edges are selected as boundary conditions due to the SHELL element type, where only the edges are used to set this kind of properties. When speaking of fixed support, what is said is that the displacement in those points are zero and the rotation is also zero. Passing these conditions to mathematical expressions to have a better understanding:

$$w(0) = 0; \quad \frac{dw(0)}{dx} = 0 \tag{74}$$

$$EI\frac{d^2w(L)}{dx^2} = 0; \quad EI\frac{d^3w(L)}{dx^3} = 0 \tag{75}$$

Where x=0 is the fixed support location and x=L is at the tip of the fin; w(x) is the displacement at the longitudinal coordinate x and dw(x) is the derivative of the displacement in the coordinate x (the first derivative is the rotation, the second one is the shear and the third is the moment). The part related to the free end is not completely equal to our model, because is not a beam and, the complexity of the inertia

and the resulting E makes it difficult to use directly in the fin's behavior (despite this, the classical theory is a good way to introduce how the fin is going to perform (Beer et al. 2003).

Continuing in the classical beam theory, which is a good approximation to have a guideline of how should the fin behave, the deflection when a local force is applied it's given by:

$$y = \frac{Px^2}{6EI}(3a - x), \qquad 0 < x < a \tag{76}$$

$$y = \frac{Pa^2}{6EI}(3x - a), \qquad a < x < L \tag{77}$$

Where the maximum deflection is given by:

$$y_{max} = \frac{Pa^2}{6EI}(3L - a) \tag{78}$$

These a and b are related with the Figure 4.12 dimensions (Beer et al. 2003).

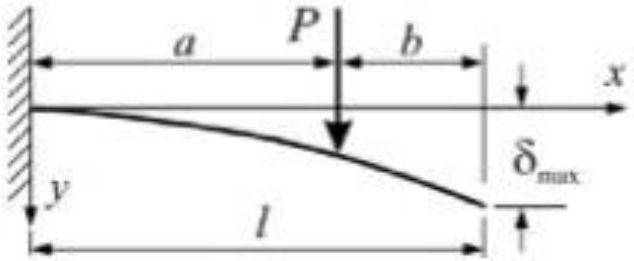

Figure 4.12- Fixed Support Beam with Punctual Force Applied

This page was intentionally left in blank.

5 Experimental Analysis

5.1 Set-up

To make the experience, it was necessary to arrange a set up that was compatible with the required boundary conditions, relating to the fin of the windsurf board. In this way, it was considered that the fin was completely fixed to the board.

The machine was calibrated on purpose for this experience. In the first try, there were errors that did not allow the experimental test to proceed, so the machine was calibrated and the errors were eliminated.

As it can be seen the Figure 5.1, the fin was fixed with long bolts that went from the bottom of the structure until box of the fin, where, using nuts, the fin was tight, replicating the fixed support of the boundary condition.

Figure 5.1- Experimental Project Set-Up

There were two main concerns with the fixing system: first, make sure that the fin was completely aligned with the block where it was settled to establish a perpendicular boundary (equal to the one observed in Figure 4.8; second, guarantee that the fin was perpendicular to cylinder that applies the force in the different locations. In Figure 5.2 it can be observed that those concerns were solved and the fin was ready to be tested.

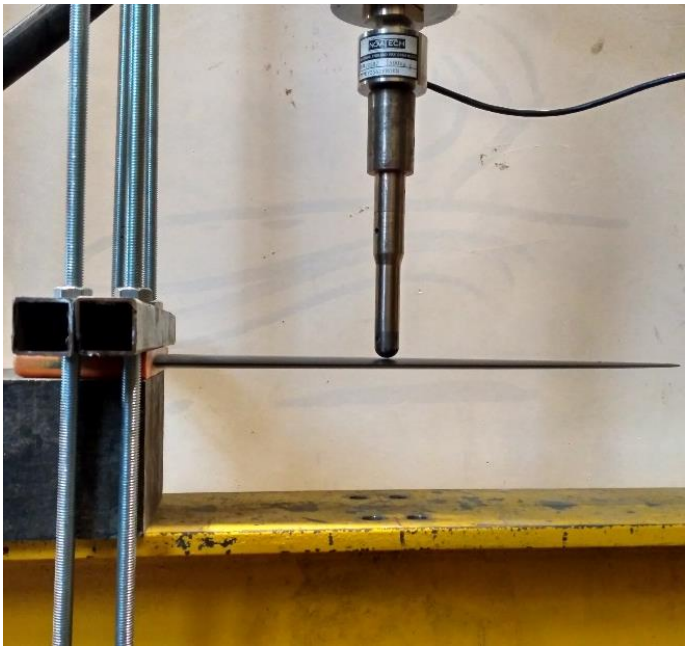

Figure 5.2- Boundary Condition

To make the test, it was used a hydraulic cylinder, fixed in the structure, above and perpendicular to the fin. The hydraulic system was controlled by a computer, where the input was the displacement of the cylinder, in this case, downwards. It was necessary to adjust to a very close position near the fin, to ensure that the values of displacement were the most absolute possible, and not too much relative to an initial position that could be far away from the fin. Attached to the cylinder, a round small piece was used (see Figure 5.3). Therefore, this ensured that the contact area was small, simulating a local force and it was not pointy, to avoid to mark permanently the fin. The possibility of slip due to large deformation was discharged because, to the point where the experience was made, the displacement was small and, both the fin and the indenter were fixed, so that possibility was liquidated. This point was also confirmed after the experiments, where the values of the rotation are small (see Figure 5.11), confirming that the option of the large displacement/rotation could be turned off, requiring less computational effort but giving also acceptable results, after the comparison between the numerical and the experimental values.

Figure 5.3- Piece to Apply Point Load

5.2 Experimental Tests and Results

To know exactly how much force and/or deflection should the fin support, a first approach in ANSYS was made, simulating the tests to give guide values until where the experimental tests should go.

Two tests were made, both on the quarter cord line: first one at 80% span, in a point weaker where fewer values of force would imply greater values of displacement and other at 40%, in a point nearer the center of the gravity of the fin as it can be seen in Figure 5.4 (the nearest point from the tip wasn't used to make any experience). In both tests, it was used a deflection's speed of 0.1mm/s.

Figure 5.4- Fin with Loading Points Marked

The hydraulic cylinder was linked to a computer which stored the data (force and deflection in the loading point) of the test.

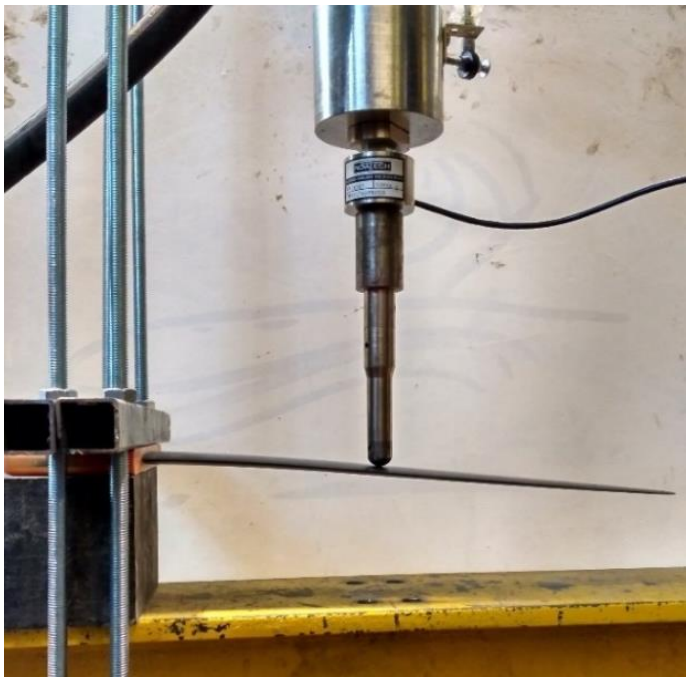

Figure 5.5- 40% Span Test

Figure 5.6- 80% Span Test

The consequent force-displacement data that came out from the tests are shown in Figure 5.7 and Figure 5.8. It can be observed that indicates that the behavior of the fin is almost linear, showing that the fin's behavior is still in the elastic domain. This is also proved, by the returning to the initial position of the fin, when the forces took off, there is no permanent deformation. Another conclusion is that, due to a higher moment and even to be in a region in fewer plies, the 80% span test requires a lot less force to present much higher deformation. This is settled by the equations (76) and (77), where the deformation is much larger as lower is the resultant Young Modulus and Inertia of the fin.

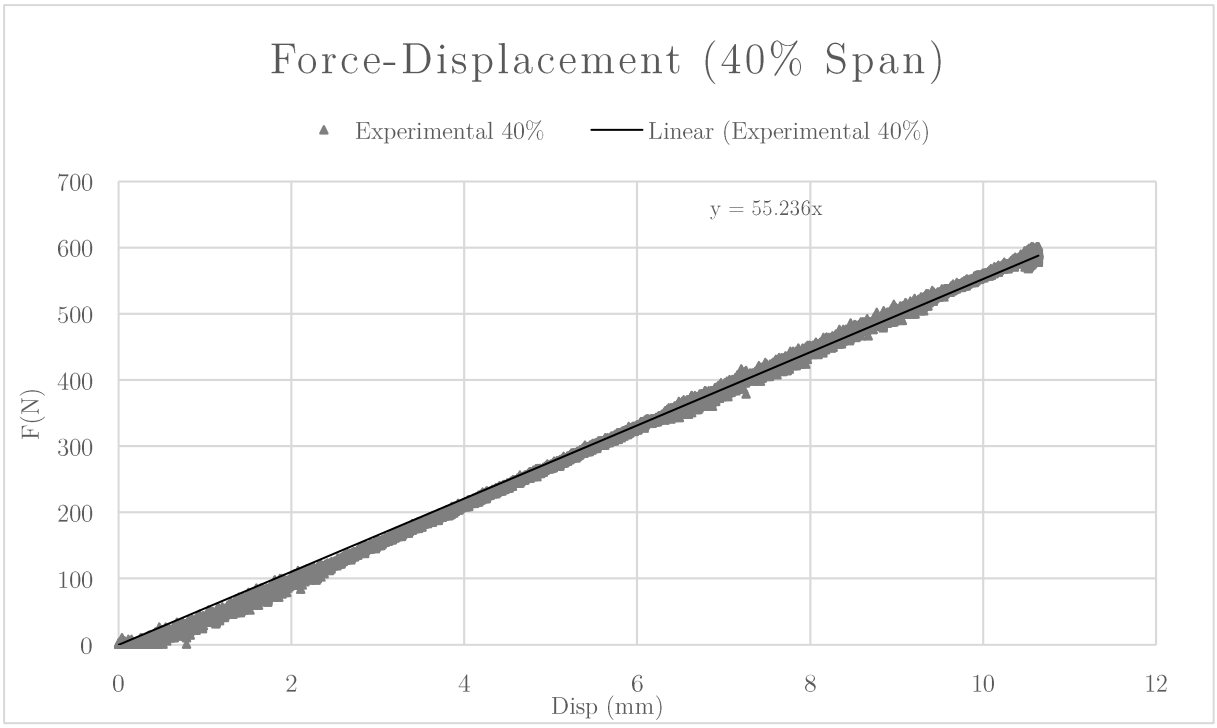

Figure 5.7- Graphic Force-Displacement (40% span)

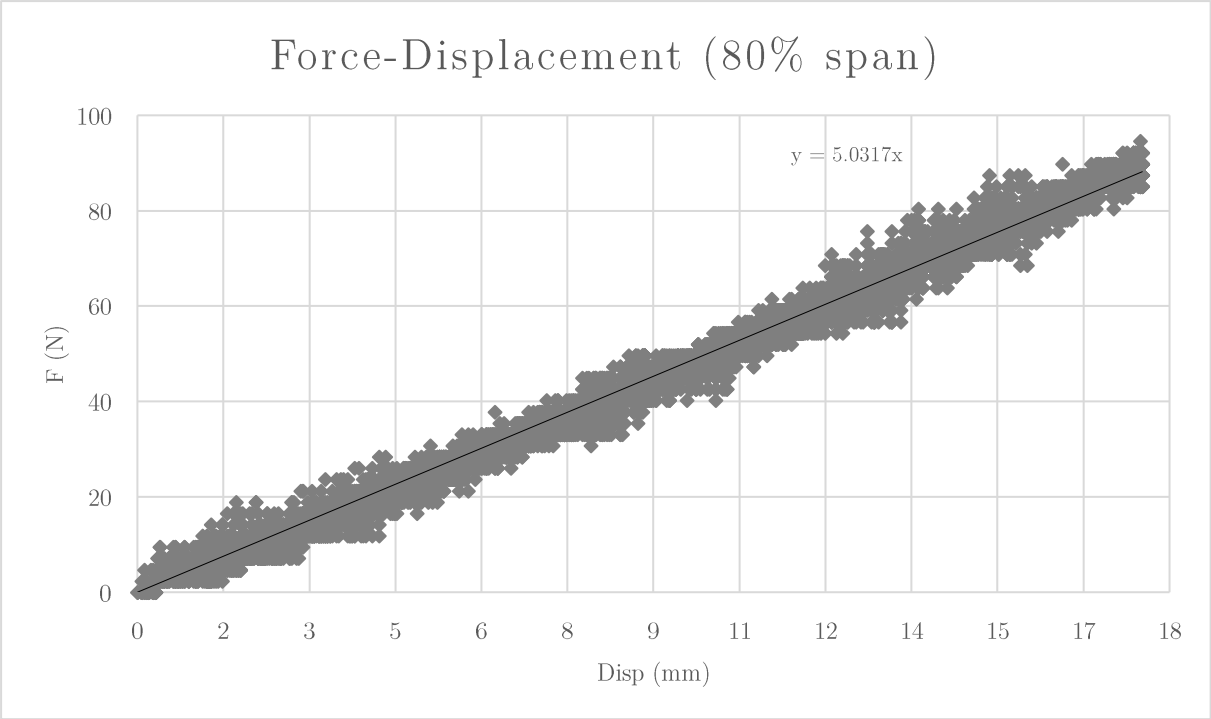

Figure 5.8- Graphic Force-Displacement (80% span)

One of the main goals of these tests was to have data to calibrate the computational model in a way that would show a similar response to the same forces.

5.3 Calibration Process

Knowing that the first values used from ANSYS library and from Miller (1991) were rather different from the final ones, it is essential to understand how this development was made.

After seeing the results, and comparing them with the previous predictions the force-displacement, it was decided that the model should be calibrated from the 40% span data, because it would be more trustable, due to the higher forces that could be applied, and due to small displacement/rotation in that point. Knowing that the tests were made only in the linear-elastic domain, one of the main properties that it was necessary to check, were the young modulus, (Timoshenko 1965):

$$E = \frac{\sigma}{\varepsilon} \tag{79}$$

Analyzing the Figure 5.7 and Figure 5.8 it was now possible to force the numerical model to behave like the real fin. The experimental data reveals, not only that the tests were made in the elastic domain but, more important than that is the fact that the behavior is highly linear. This property revealed by the data implies that, the calibration process should be to adjust the slope of the force-displacement curve until fits almost perfectly to the obtained in the experimental tests. In this way, the young moduli of the material properties that were used in input values were readjusted to give the model better results. Some other processes could be adopted but this one was selected in the way that, it was the easiest, quickest and the safest one.

There were three types of fibres that could be adjusted: unidirectional carbon fibres, multidirectional carbon fibres and unidirectional glass fibres. First, it was necessary to maintain the relation between the values and their respective directions, meaning that in the multidirectional fibres, E_x and E_y should have equal values and in the unidirectional ones, E_y and E_z were the ones that should be equal. A second important topic was that, in each fibre, the relation (increasing or decreasing in relation to the initial value) was made equally in all directions. This means that a 10% increase was made in the unidirectional fibre in relation to the initial value, this was made in all the directions, knowing that E_y and E_z were the ones that should be equal as explained. The initial young moduli values were obtained from ANSYS library and can be observed in Table 5-1.

Table 5-1- Young Modulus Initial Values (Ansys Library)

	Units	Epoxy Carbon UD	Epoxy Carbon Woven	Epoxy E-Glass UD
$\mathbf{E_x}$	MPa	1.21E+05	61340	45000
$\mathbf{E_y}$	MPa	8600	61340	10000
$\mathbf{E_z}$	MPa	8600	6900	10000

These initial input values were used to initiate the calibration process. In this way, the first simulation at 40% of span and a quarter of the chord from the leading-edge lead to the result shown at Figure 5.9.

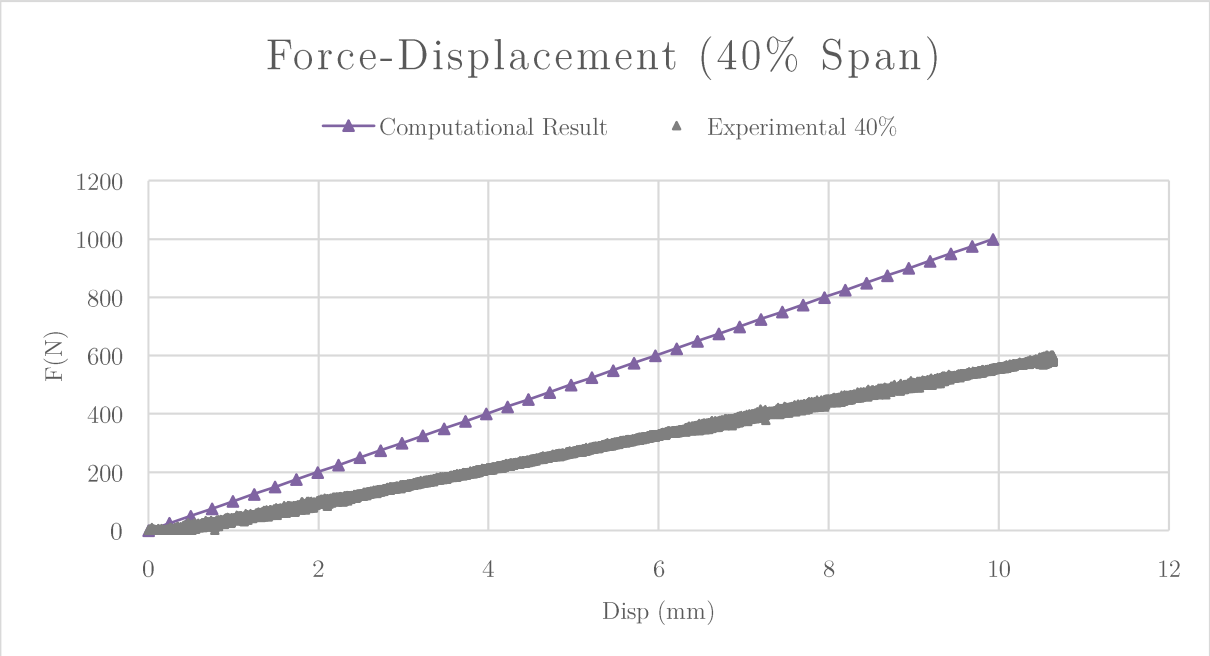

Figure 5.9- Graphic Force- Displacement (40% Span)- Experimental vs FEA Model with initial ANSYS Young Moduli values

This first approach indicates that the numerical model is more strength than it should be, compared with the real fin. In this way, it was necessary to reduce the values of the young moduli of the fibres, although this process needed to be taken with precaution to maintain the rigid structure of the fin. After some tests, one of the main conclusions was that, the plies that occupy more area of the fin, should be reduced less in order to maintain the linear behavior. This is even more evident because the e-glass fibres are displaced in a central region almost at 50% of the span. If this fibres had greater values compared to the carbon ones, it would lead to a break at the end of the e-glass fibres (this break would be completely unreal compared to the theoretical breaking point).

To calibrate the numerical model, all three values of young moduli were reduced and the final values were obtained by trial and error, maintaining the initial proportions and the relations concerning the type (unidirectional or multidirectional). The values can be observed in Table 5-2 and the resulting comparison between the data obtained from the experimental tests and the behavior of the numerical model can be observed in Figure 5.10.

Table 5-2- Final Values of Young Moduli of the Fibres

	Units	Epoxy Carbon UD	Epoxy Carbon Woven	Epoxy E-Glass UD
$\mathbf{E_x}$	MPa	58606	30670	12000
$\mathbf{E_y}$	MPa	2413	30670	2668
$\mathbf{E_z}$	MPa	2413	3450	2668

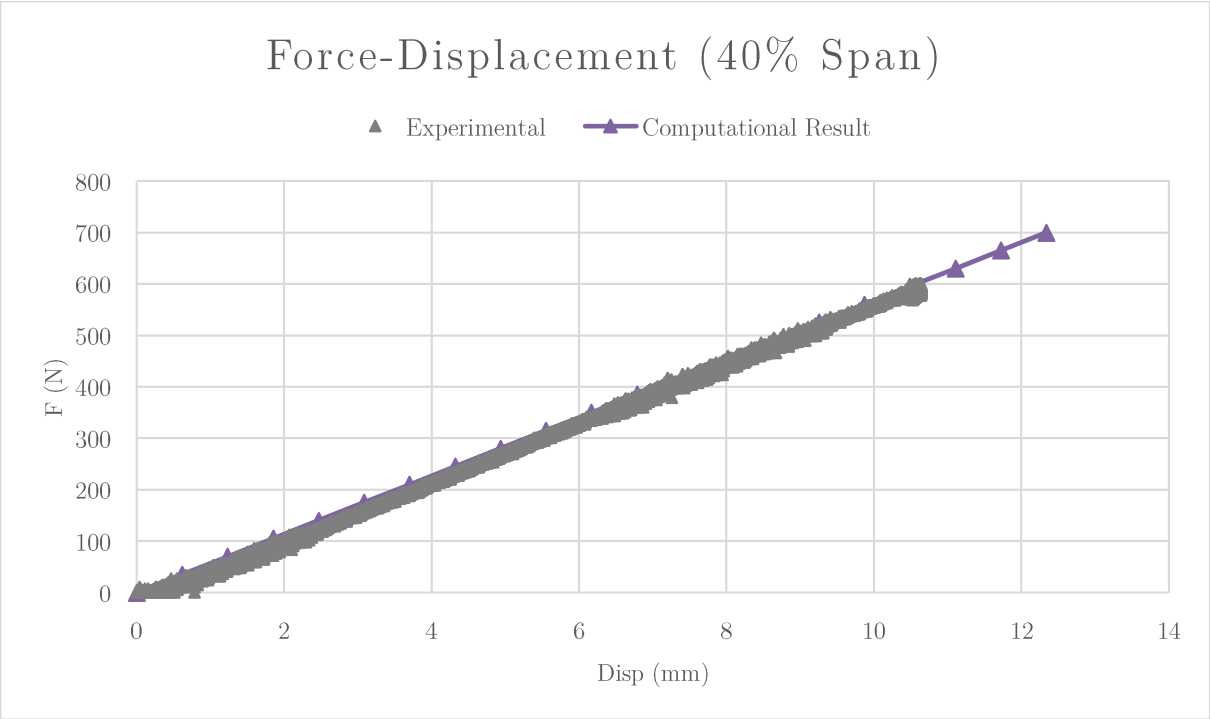

Figure 5.10- Graphic Force- Displacement (40% Span)- Experimental vs FEA Model

As it can be observed in Figure 5.10, the numerical model follows up closely the behavior of the real fin, demonstrating that the model created in ANSYS is trustable, although safety margins are always required. With this first verification, it is necessary to verify if the large deformation option could be turned off in ANSYS. This is usually a major source of problems, giving, in most of the times, problems of convergence and, as results, problems in the accuracy of the results. To check this, it was made a graphic Moment-Rotation to evaluate the values of rotation in the point of the applied load. The moment is calculated by the following formula:

$$M = F.d \tag{80}$$

where d is the perpendicular distance to the fixed support. The value, in meters, for the distance is 0.144m.

Knowing this, and looking at the same range of the computational simulation in Figure 5.10, the results are shown in Figure 5.11. With this information, it is possible to understand that the large deformation could be turned off, not only because of the small values of rotation, but also because this option turns on a great package of non-linearities and, like it can be observed in Figure 5.7, the fin follows up a high linear behavior.

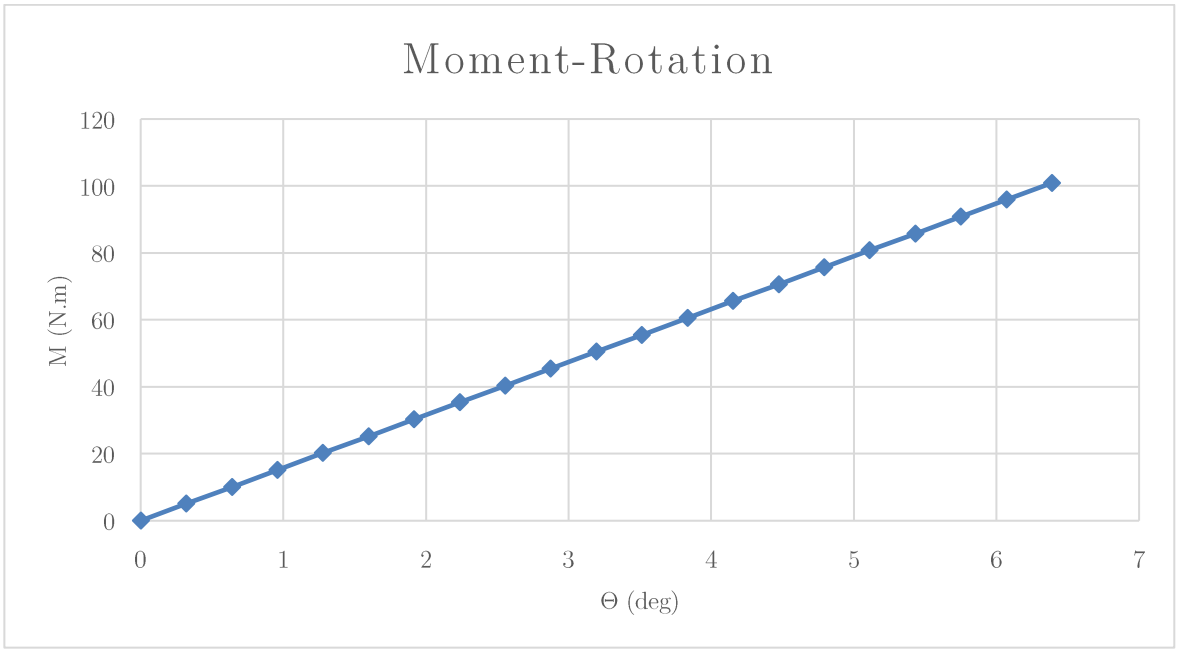

Figure 5.11- Graphic Moment-Rotation

Despite these values, there was an effort to have the large displacement option turned on, to understand if it there was any sense in it. Some tests were made and, due to severe convergence problems, the finest evaluation graphic that came out was the one that can be observed in Figure 5.12.

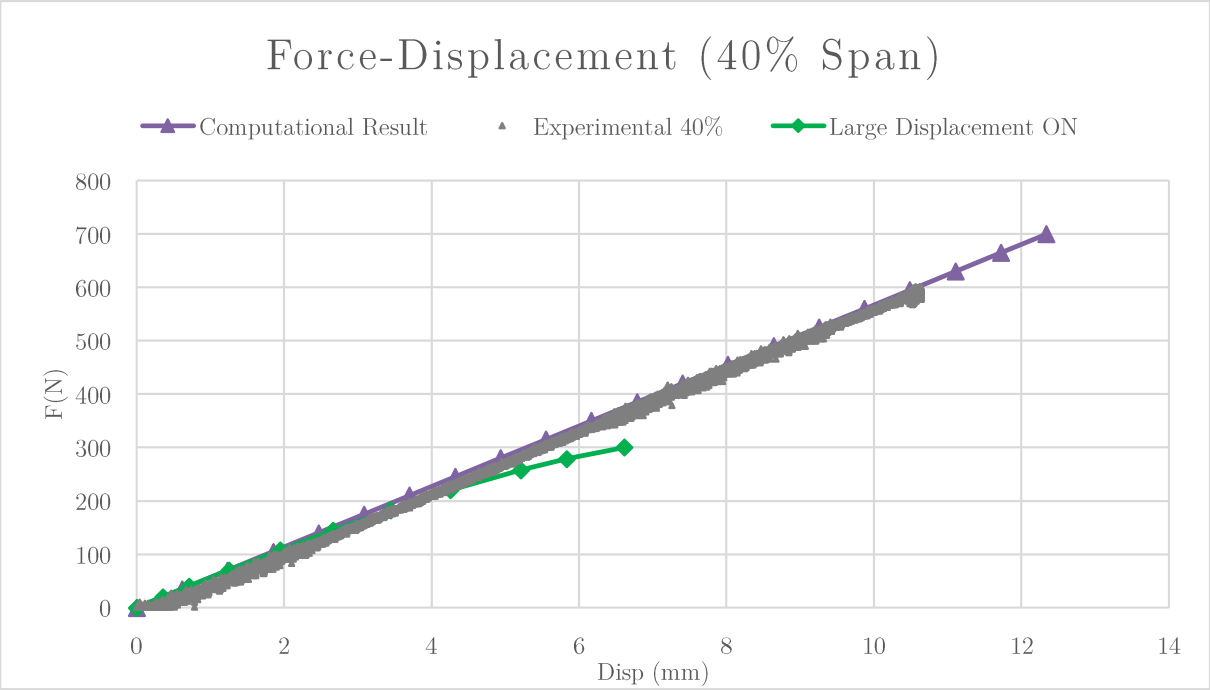

Figure 5.12- Comparison Large Displacement ON

As it can be observed in Figure 5.12, when the option large displacement is turned on, the behavior starts to be very nonlinear after 200N and, does not converge beyond 300N. Knowing all this, the large displacement option was turned off.

It is important to make a global analysis of the fin. This means that the analysis should not only be at the loading point, it should be at all the model. To make this analysis, and even to go to the failure predictions, the force applied was increased until 2500N. Most of the results shown here will have different values of force (the values will be explicit in each case).

Figure 5.13 shows one of the most important graphics in the analysis of the ultimate strength. Moment-Curvature analysis is a method to determine the load-deformations behaviour of a concrete section using nonlinear material stress-strain relationships. For a given axial load, exists compression fibre strain and a section curvature **k** at which the nonlinear stress distribution is in equilibrium with the applied axial load. A unique bending moment can be calculated at this section curvature from the stress distribution. Deriving the curvature (Beer et al. 2003):

$$k = \frac{1}{\rho} \tag{81}$$

and:

$$k = \frac{1}{\rho} = \frac{d\theta}{ds} \tag{82}$$

Considering B as the application point of the force, A the fixed support point:

$$d\theta \approx \Delta\theta = \theta_B - \theta_A = \theta_B - 0 = \theta_B \tag{83}$$

and

$$ds \approx \Delta s = \sqrt{(x_B - x_A)^2 + (v_B)^2} \tag{84}$$

Resulting into:

$$k = \frac{\theta_B}{\sqrt{l^2 + v_B^2}} \tag{85}$$

where v_B is the vertical deflection in the application point, θ_B is the rotation (in radians) at point B and l is the longitudinal distance from point A to B.

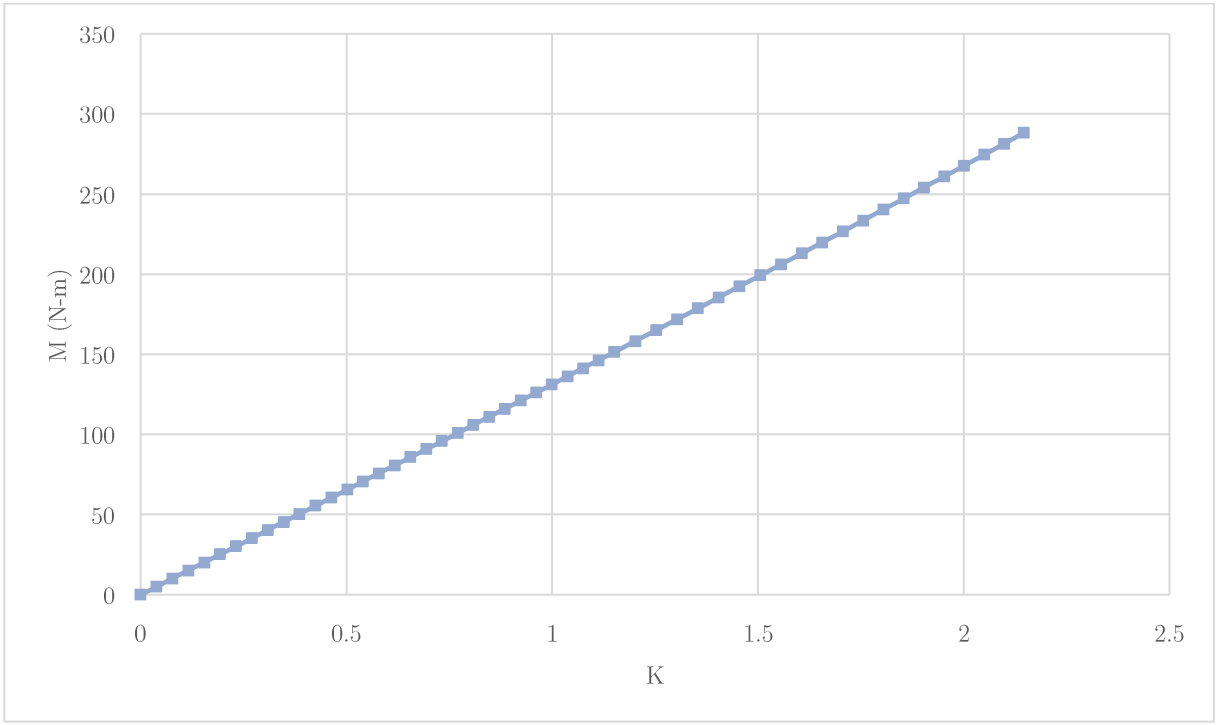

Figure 5.13- Moment-Curvature

Starting with the deformation, it is expected that the maximum deformation occurs in the tip of the fin. In this case, Figure 5.14 shows de deformation for 1000N. It is represented also the non-deformed shape. Observing Figure 5.14, the deformation as it maximum value at the tip (where the x value is equal to the span of the fin), as it was expected by the equation (78), when the x value was equaled to the longitudinal dimension L.

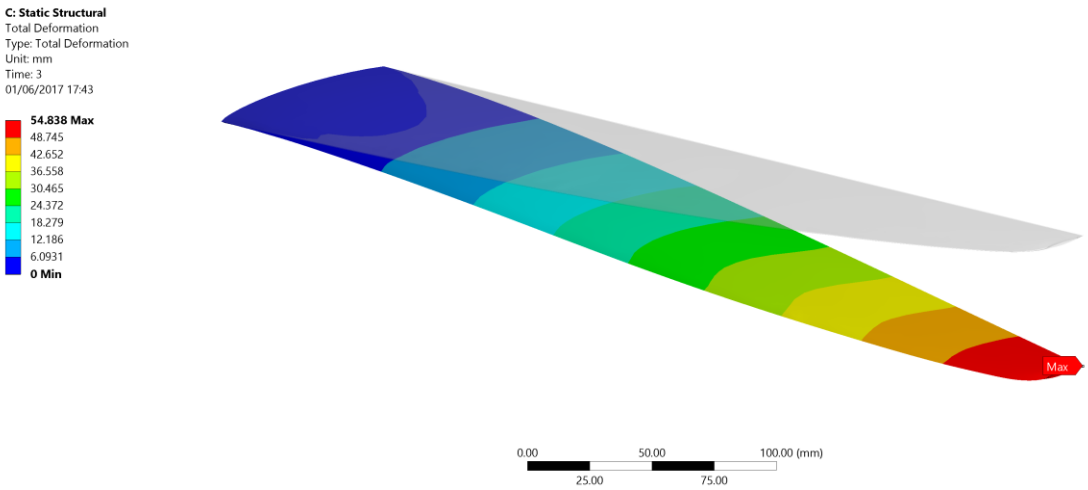

Figure 5.14- Deformation (1000N)

One of the other important results that need to be analyzed is the distribution of the stresses. Due to its fixed support, it is expected to have higher stresses near the support. Figure 5.15 is also representative of a 1000N load applied and are represented the maximum principal stresses.

Like predicted, the higher stresses occur near the fixed support, where the fin concentrates most of its stresses. These results can lead to an estimate that, when the fin will break, it should be near the support, due to the accumulation of stresses that will lead to a complete failure. This point is explained by the Figure 4.8 and its consequent equations of the distribution of shear and bending moments. This implies that, it is predictable that when observing the shear stresses, higher values are expected near the boundary fixed condition.

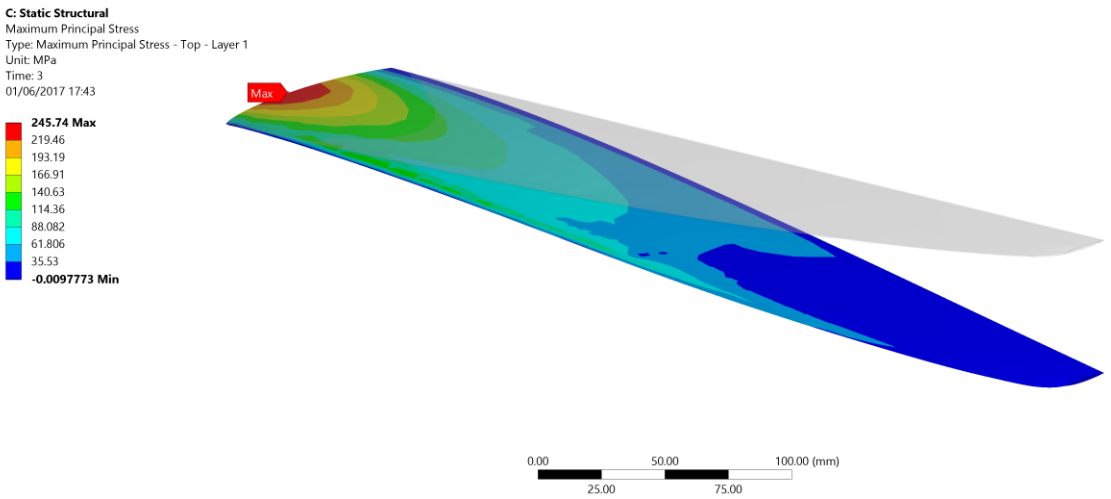

Figure 5.15- Distribution of Maximum Principal Stresses (1000N)

In this way, one of other important stresses that need to be analyzed is the shear stress. It is represented the distribution of shear stresses when applying a load of 1500N in Figure 5.16. These shear stresses are not the interlaminar shear stresses, but are the ones induced by the vertical remote force.

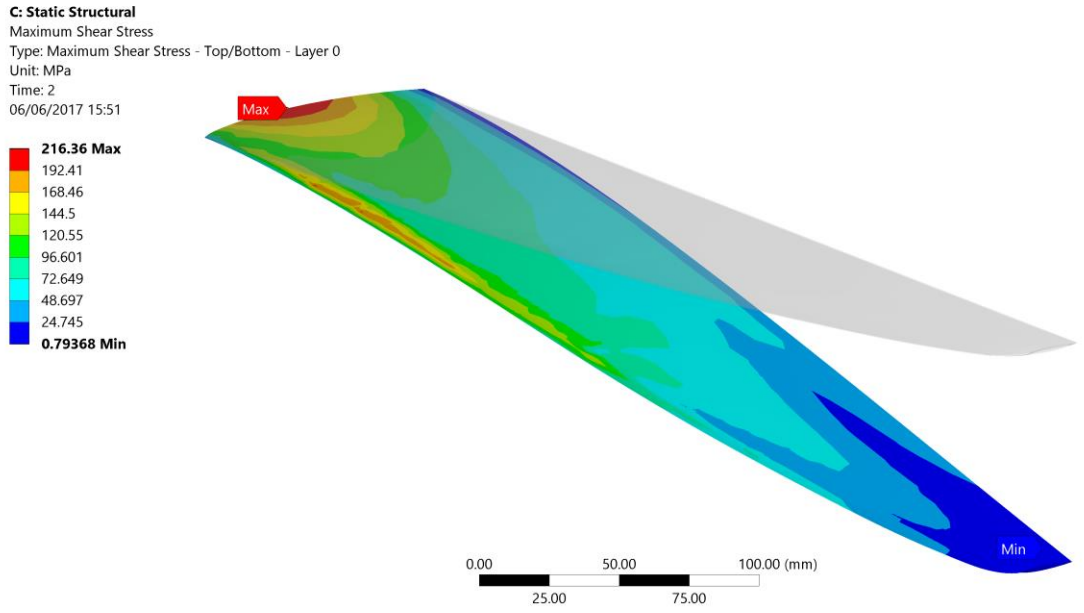

Figure 5.16- Distribution of Maximum Shear Stresses (1500N)

When talking about static structural problems, an object is in equilibrium when each point inside the object has the same constant velocity (generally, velocity is zero for static's problems). Therefore, an object in equilibrium is not experiencing any accelerations, so Newton's 2nd Law can be written as:

$$\sum F_i = m.a = 0 \tag{86}$$

In this case, the force applied should be equal to the reaction force. The check-up was made and the results proved that the requirement was accomplished. Although the applied force is in the z direction, some residual forces appear in other directions, but in the final, the sum of all them is equal to the applied force (example with until 1500N).

In Figure 5.17, the upper line is the evolution of the applied force and the other line is the consequent reaction force. As it can be seen, the reaction forces equal in every instant the force applied, accomplishing the equation (86).

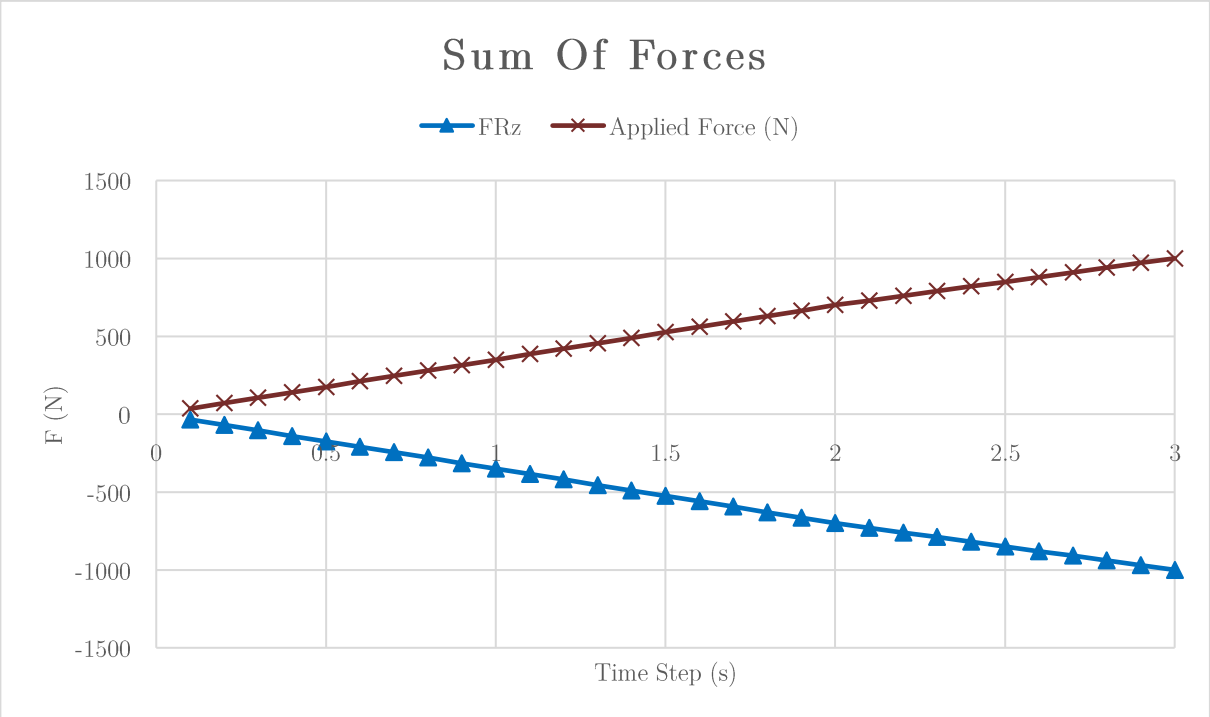

Figure 5.17- Force Reaction

This page was intentionally left in blank.

6 Failure Analysis

6.1 Introduction

Most experimental results of material strength, properties are based on uniaxial tests. Despite this, when talking about composite structures, multi-axial stress states are present and it is very important to predict the failure in all these different stress states (W Van Paepegem and Degrieck 2003).

Although multi-axial stress states should be prevented, it is also very important to analyze the type of materials that are used in the composite structures. In this way, most of the materials used are anisotropic. These anisotropic materials are materials whose properties are directionally dependent, which is the complete opposite to the isotropic materials, where the material properties are equal despite the orientation. This characteristic is one of the major sources of errors between the computational models and the real ones because the shipyards develop their own ways to apply the fibres and resins, and the final properties will change, leading to different results in the propagation of the stresses and the consequent deformations (Christensen 2008).

To prevent these different properties and all the different points discussed in the sub-chapter 3.1 Composite Materials, and because in this dissertation it does not need to associate the failure to the failure modes (fibre fracture, transverse matrix cracking and shear matrix cracking for example), only the failure criterion proposed by Tsai and Wu (1971) will be considered (some predictions about fiber failures will be put into consideration just to have some guide values to future work). In this main group of failure criteria not associated with the failure modes, the Tsai-Wu it is one of the most important ones as reported by Camanho (2002). This impossibility of predicting the failure mode is not important because the windsurf fins used in competition are not made to be used with internal cracks or small lamina failures, so this constraint is not a problem. Nevertheless, a prediction of the fibre failure will be made, using the postprocessor in ANSYS (knowing that this is not the main failure criterion in this dissertation).

6.2 Application

The calibration of the FE model is to be done with the data obtained from the experimental results. Like explained in this chapter, the main failure criterion is the Tsai and Wu (1971) but it is going to be also used a maximum stress criterion, just for the fibre failure.

The application of this criterion was completely from the ANSYS ACP postprocessor. It is a tool where, after the loads are applied, the results are discriminated and are evaluated, applying some criteria (see Figure 6.1)

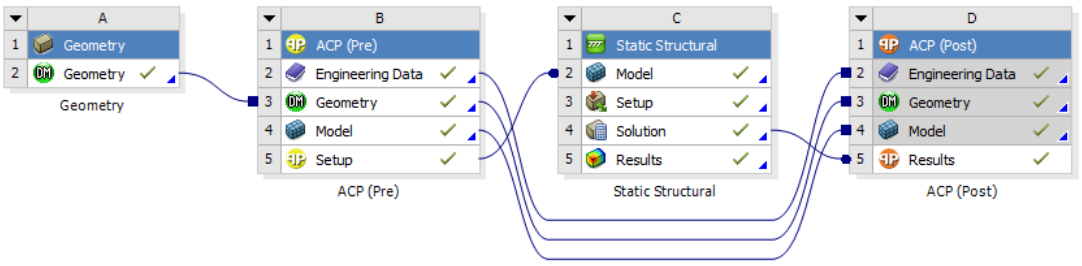

Figure 6.1- ANSYS Workbench GUI

Both criteria will be analyzed from ply to ply, although the Tsai-Wu does not specify the failure mode, and so, it could be a failure in the resin or even a shear failure. What is expected is that the Tsai-Wu criterion will present failure much sooner than the fibre failure, which is one of the last failures to occur in composite laminates.

So, starting with the Tsai-Wu criterion, it was necessary to search for the value where a ply presents a value over one, as stated in Equation (40). After the analysis, the value of the force that produces a first ply failure is 910N in the 1st ply that is under compression, showing a factor above 1 (1.0307), which indicates failure as explained by the Equation (32).

As it can be observed in Figure 6.2, the higher values are near the fixed support. It is also observed a higher stress small region near the leading edge at the half of the span, but that should be ignored because it is possible to be due to a modelling error.

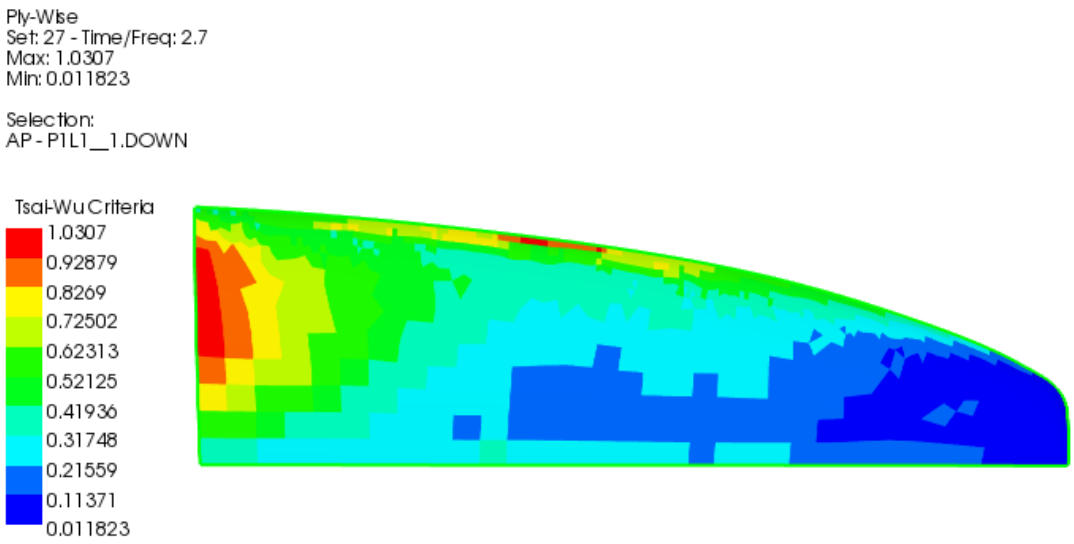

Figure 6.2- Tsai-Wu Failure

Although Tsai-Wu criterion presents trustable values, does not tells what kind of failure occurs. Knowing that information is not the most important in the goals of the project, the possibility to have a prediction of a failure criteria associated with the failure modes, is way to understand better the real behavior of the fin. These criteria consider that the non-homogeneous character of composites leads different failure modes of the constituents. The criteria are established using mathematical expressions, considering material strengths and strains limits. The criteria that are going to be analyzed are the Maximum Stress Criterion and Maximum Strain Criterion.

Starting with the first one, it considers that the composite fails when the stress exceeds the respective allowable. Is a simple and direct way to predict failure in composites and no interaction between the stresses acting on the lamina are considered. Three different conditions of failure are considered, although in this project only the failure of the fibres is going to be analyzed (Camanho 2002):

$$\textit{Fibre}: \quad \sigma_1 \geq \sigma_{1T}^u \quad or \quad |\sigma_1| \geq \sigma_{1C}^u \tag{87}$$

$$\textit{Matrix}: \quad \sigma_2 \geq \sigma_{2T}^u \quad or \quad |\sigma_2| \geq \sigma_{2C}^u \tag{88}$$

$$\textit{Shear}: \quad |\sigma_{12}| \geq \sigma_{12}^u \tag{89}$$

Studying the fibre failure, the values of the required force are, necessarily, higher. The results shown in Figure 6.3, proved this, explicating that the necessary force was 2050N, where the failure factor is above 1 (1.018), also near the fixed support part of the fin, like expected. This occurs in the compressive part of the fin (specifically in 4.DOWN ply)

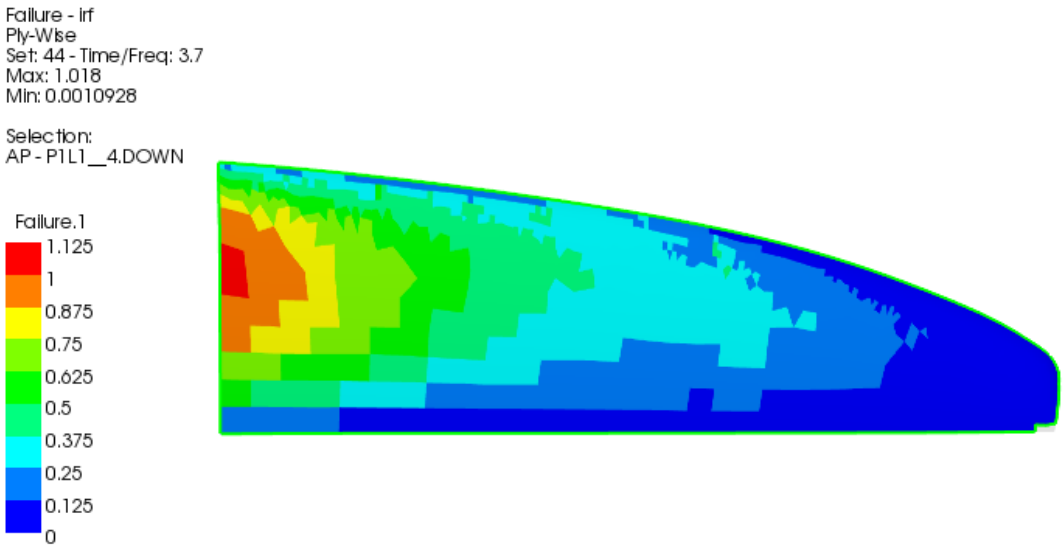

Figure 6.3- Fibre Failure- Maximum Stress Criterion

Moving to the second criterion: Maximum Strain Criterion. It is considered that the composite fails when the strain exceeds the respective allowable, being also a simple and direct way to predict failure of composites. Again, three different conditions are considered in correspondence with a maximum strain fibre direction, matrix or transversal direction and for shear strains (Camanho 2002):

$$\textit{Fibre}: \quad \varepsilon_1 \geq \varepsilon_{1T}^u \quad or \quad |\varepsilon_1| \geq \varepsilon_{1C}^u \tag{90}$$

$$\textit{Matrix}: \quad \varepsilon_2 \geq \varepsilon_{2T}^u \quad or \quad |\varepsilon_2| \geq \varepsilon_{2C}^u \tag{91}$$

$$\textit{Shear}: \quad |\sigma_{12}| \geq \sigma_{12}^u \tag{92}$$

Figure 6.4 displays that the failure occurs also in the compressive side (ply 4.DOWN) when the force reaches a value of 825 N.

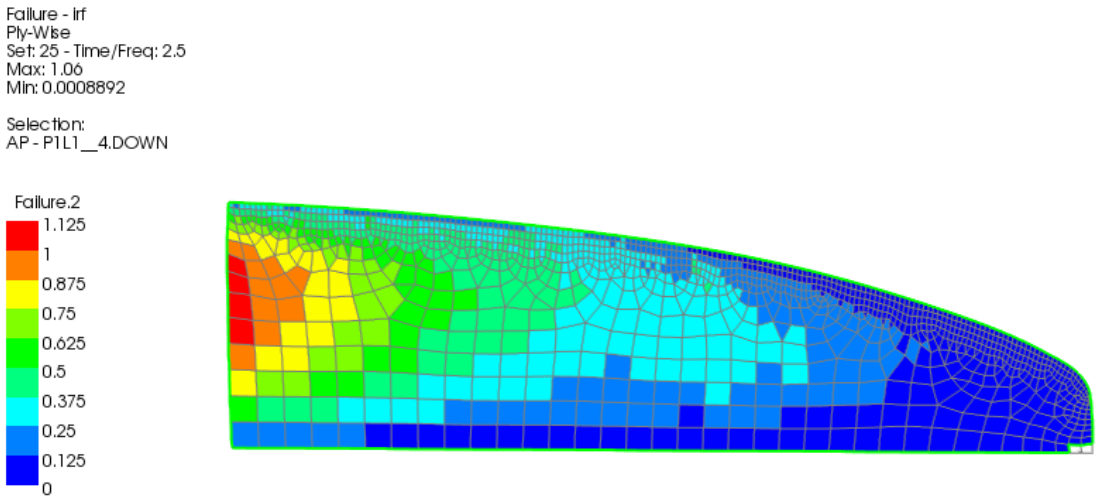

Figure 6.4- Fibre Failure- Maximum Strain Criterion

Another criterion that was observed was the combined one, between the maximum stress and the maximum strain. Despite being also only for fibre failure, this is a more conservative approach because only implies a failure of one component (reach maximum stress or strain in each fibre) and detect a failure in the ply.

This last criterion shows a failure in the same ply (4.DOWN- under compression) but, in this case, the required value to have failure dropped to 820N. This is highly conservative, but it necessary to do it, to keep the safety margins at a good level due to the complexity of replicating a real model in a computational one. The results can be seen in Figure 6.5.

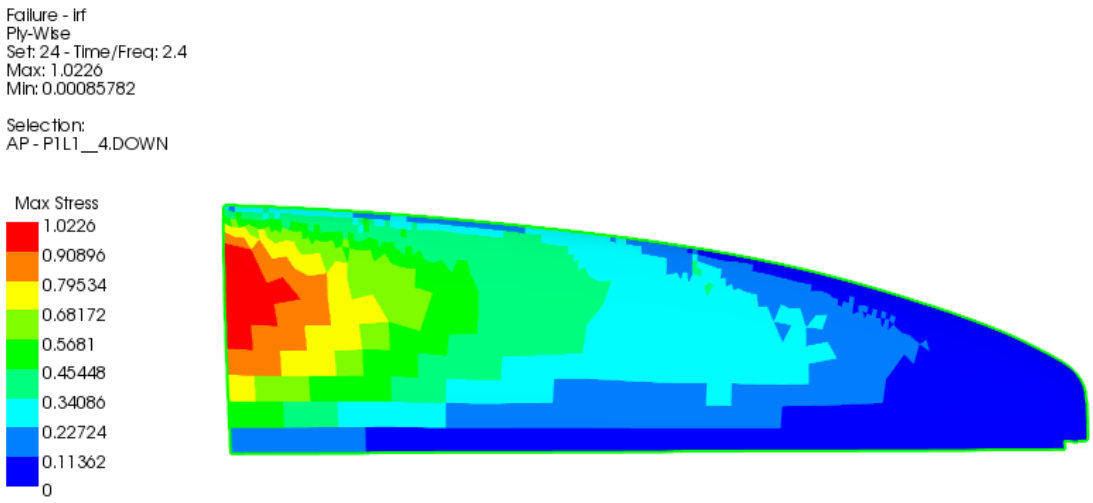

Figure 6.5- Fibre Failure- Maximum Stress & Strain Criterion

Resuming all these failure criteria values (not including the combined of maximum stress and strain criterion), relating the forces, deflections and maximum stresses in one single table, the results can be observed in Table 6-1.

Analyzing the values, the first failure criterion that is full-filled is the maximum strain. This indicates that the fibres start to stretch more that they should but, despite this, the great difference between this value and the maximum stress values also indicate also that it could be the data of the maximum strain values of the materials that it is not properly fit to the reality of the fin. These values would be good ones if the analysis would be focusing on the failure of the matix, that requires much lower values to fail, as the Tsai-Wu failure criterion seems to indicate. This criterion is achieved with a relatively low value of force, which naturally indicates that the failure is in the matrix (although this is only a prediction since Tsai-Wu criterion does not indicate what is the failure mode as explained before).

Table 6-1 also demonstrates that, all criteria shows failure in plies that are under compression. This result is expected, since, when analyzing the orthotropic stress limits, the values that are for tension are (in absolute value) higher than the compression ones. When considering equal plies, subjected to the same forces in the same conditions, the compression ones will fail first because they have lower values of stress limits.

Table 6-1- Failure Criteria

Failure Criterion	**Force (N)**	**Ply Failure**	**Maximum Deflection (mm)**	**Maximum Stress (MPa)**
Tsai-Wu	910	1.DOWN	49.902	223.62
Max Stress	2050	4.DOWN	109.68	393.18
Max Strain	825	4.DOWN	40.031	201.51

It is not obvious the type of relation between the maximum stress and the deflection. When observing Figure 6.6, it shows that it is not completely linear, suggesting that, if the experimental tests were made until the fin breaks, after some time, the fin would have a more non-linear behave due to internal cracks, not only in the fibres but, especially in the matrix. The maximum stress and strain are related only with fibre failure.

The decrease of the slope indicates that, with the increase of the force (and the consequent stress), the fin will deflect easier, revealing the higher non-linearities, that could only be confirmed with an experimental test that would go until the fin breaks.

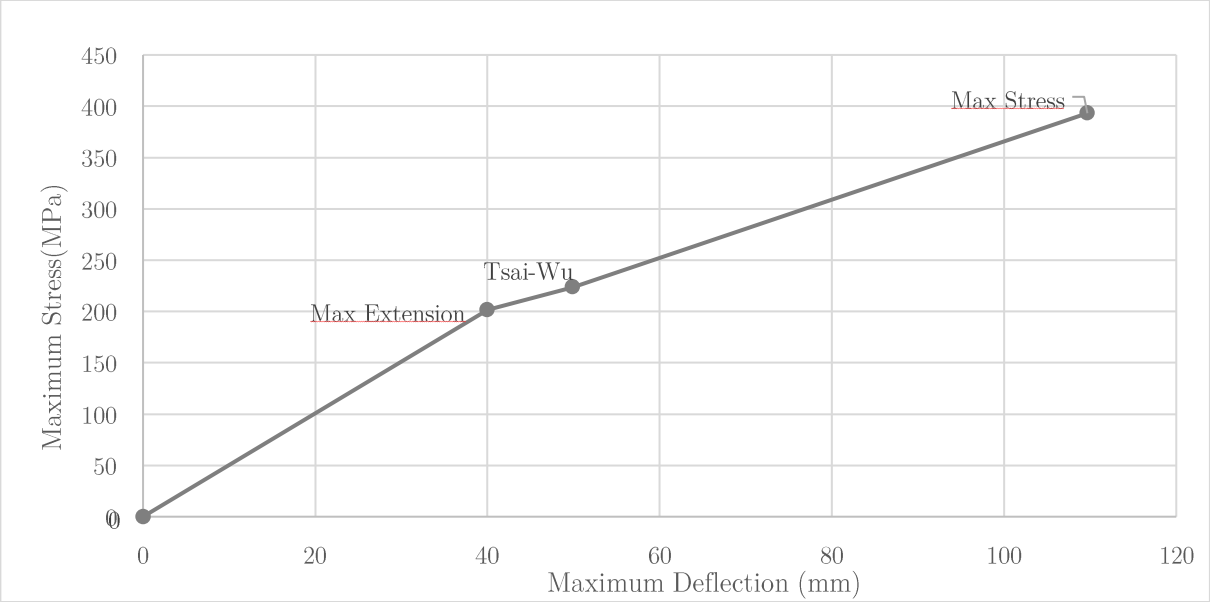

Figure 6.6- Stress vs Deflection (Comparison Between Failure Modes)

This page was intentionally left in blank.

7 Conclusions

The initial objectives of this project were "to create a numerical model of a windsurf fin, analyzing its ultimate strength. This numerical model is to be calibrated by the data obtained in the laboratory, where a real-scale model is to be tested."

The objectives were completed during the working process, wherever talking of the initial research, the creation of the model, the experimental tests, the consequent calibration or the predictions of failure of the fin with the creation of a numerical model that can be trusted (by the demonstration of similar behavior when compared with the real-scale model).

7.1 Results

Although the project does not have a large domain of results, this is explained by being a first approach in this area in CENTEC, with the necessity of exploring much more before having the results. The construction of a trustable computational model which is capable of being used in further projects was one of the most important parts of this project. For this to happen, it was necessary to talk with some experts in composites, research and even with all this knowledge, it was necessary to adjust the FE model. In the composite area, information like material properties is not very spread, making the experience and internal knowledge a well-kept secret, but also making very difficult to advance in this type of projects.

The results of displacement were very accurate, with the model created in ANSYS 18 Workbench retrieving values of deformation very close to the ones obtained in the experimental test. It shows a highly linear performance, predicting a very short plastic domain until the fin breaks.

In the failure modes, the application of the different criteria was very important to understand that the fail can occur in very different ways. The Tsai-Wu failure criterion cannot predict what is the failure mode but, due to its low value of failure mode, it is more probable that is associated with cracks in the matrix (resin) because, when analyzing the failure of maximum stress of the fibres, the values of the force are much higher than the ones presented by Tsai-Wu criterion.

7.2 Future Works

The innovative application of FEM analysis to the nautical sports bodies in composites has an enormous space of progression, making this the first work in the domain of the analysis of a windsurf fin in CENTEC. This first approach, with the model of the fin done and calibrated, allows future works could move faster and for deeper fields, moving ahead to other important domains where the performance of the fins could improve relatively easier.

The creation of a valid and calibrated numerical model, capable of predict the structural behavior of the fin is the powerful tool in future works in deeper fields of analysis. In terms of future work hypothesis, it would be very important to make an experimental test until the fin breaks. This would give a complete spectrum of the behavior, and the capacity of understanding in each gamma of values should the model resist. This test would also give data about its plastic domain, that, although the predictions indicate that has a very small plastic domain, it would be important to confirm the predictions with experimental tests. It would be also interesting to make tests of dynamic loads, to adjust better the model to a real fin, due to the fact the piece is in constant changes of direction so the loads are not even quasi-static. The disposition of the plies and even the type of the fibres applied could be also tested, applying different fabrics, changing the lay-up disposition and comparing the results to obtain the optimized model in terms of structural response. Another field that could be important is the CFD analysis. This hydrodynamic shape could be studied and, if possible or necessary, optimized for better results.

8 Bibliography

Ansys Inc. (n.d.). 4.181 SHELL181 Finite Strain Shell. http://ans2.vm.stuba.sk/html/elem_55/chapter4/ES4-181.htm. Accessed 31 May 2017

Ansys Inc. (2013). *ANSYS Mechanical APDL Modeling and Meshing Guide*. Canonsburg. http://www.ansys.com. Accessed 3 February 2017

Barbero, E. J. (2008a). *Finite Element Analysis of Composite Materials Using ANSYS* (2nd Edition). CRC Press.

Barbero, E. J. (2008b). *Finite Element Analysis of Composite Materials* (2nd Edition). CRC Press. doi:10.1533/9781845692537.46

Barbero, E. J. (2010). *Introduction to Composite Materials Design* (2nd Edition.). CRC Press.

Beer, F., Johnston, E. R., & Dewolf, J. T. (2003). *Mecânica dos Materiais* (3th Edition). Lisboa: McGraw Hill.

Bogucki, G., McCarvill, W., Ward, S., & Tomblin, J. (2003). Guidelines for the Development of Process Specifications, Instructions, and Controls for the Fabrication of Fiber-Reinforced Polymer Composites, (March), 48. http://www.tc.faa.gov/its/worldpac/techrpt/ar02-110.pdf

Bureau Veritas. (2012). Hull in Composite Materials and Plywood, Material Approval, Design Principles, Construction and Survey, *33*(546).

Callister, W., & Rethwisch, D. (2007). *Materials Science and Engineering: An Introduction. Materials Science and Engineering* (7th Edition, Vol. 94). John Wiley & Sons, INc. doi:10.1016/0025-5416(87)90343-0

Camanho, P. (2002). Failure criteria for fibre-reinforced polymer composites. *Demegi, FEUP*, 1–13. doi:10.1016/j.compscitech.2014.05.033

Christensen, R. M. (2008). Failure Criteria for Anisotropic Fiber Composite Materials.

Clouston, P., Lam, F., & Barrett, J. D. (1998). Interaction Term of Tsai-Wu Theory for Laminated Veneer. *Journal of Materials in Civil Engineering*, *10*(May), 112–116.

Exel. (2016). Exel- Raw Materials- Reinforcements. http://www.exelcomposites.com/en-us/english/composites/rawmaterials/reinforcements.aspx. Accessed 24 April 2017

Fagg, S. (1997). The development of a reversible and finitely variable camber windsurf fin. *Vasa*, (September). http://eprints.bournemouth.ac.uk/12235/

Gere, J. M., & Timoshenko, S. P. (1991). *Mechanics of Materials*. doi:10.1007/978-1-4899-3124-5

Greene, E. (1999). *Marine Composites Second Edition*. *Marine Composites (2nd Edition)*. doi:10.1016/0010-4361(78)90325-7

Gurit Holding AG. (2000). Guide to Composites. doi:GTC-3-0509

Hexcel. (2013). HexPly Prepreg Technology. *Hexcel Registered Trademark*, 28.

Kelly, P. (2015). Anisotropic Elasticity. In *Solid Mechanics Part I* (pp. 153–166).

Matthews, F., Davies, G., Hitchings, D., & Soutis, C. (2000). *Finite element modelling of composite materials and structures*. (CRC Press, Ed.)*Woodhead Publishing Limited* (1st Edition). Woodhead Publishing Limited.

Miller, P. . (1991). *NNS composite materials properties database, unpublished composite test program report*.

Narayanaswami, R., & Adelman, H. M. (1977). Evaluation of the Tensor Polynomial and Hoffman Strength Theories for Composite Materials. *Journal of Composite Materials* . doi:10.1177/002199837701100401

Nowakowska, B., Colino, B., Yeter, B., & Tekgoz, M. (2011). *Modeling of a Composites Windsurfer Fin*. Lisboa.

Paepegem, W. Van. (2002). *Development and finite element implementation of a damage model for fatigue of fibre-reinforced polymers*. http://hdl.handle.net/1854/LU-153455

Paepegem, W. Van, & Degrieck, J. (2003). Calculation of Damage-dependent Directional Failure Indices from the Tsai-Wu Static Failure Criterion. *Composites Science and Technology*, *63*(2), 305–310.

Pinho, S. T. (2005). *Critérios de Rotura de Materiais Compósitos*. Porto.

Raby, A. (2011). Choosing Your Windsurfing Fin. http://www.mariner-sails.com/archives/Choosing Your Windsurfing Fin.pdf. Accessed 6 July 2017

Rusmee, P. (2014). High Strength Composites.

Savoia, M., & Tullini, N. (1996). Beam theory for strongly orthotropic materials. *International Journal of Solids and Structures*, *33*(17), 2459–2484. doi:10.1016/0020-7683(95)00163-8

Shenoi, R. A., & Wellicome, J. F. (1993). *Composite Materials in Maritime Structures, Volume 1 Fundamental Aspects*. Southampton.

Silvestre, N., & Camotim, D. (2002). Second-order generalised beam theory for arbitrary orthotropic materials. *Thin-Walled Structures*, *40*(9), 791–820. doi:10.1016/S0263-8231(02)00026-5

Sutherland, L. S. (1993). *Windsurfer Fin Hydrodynamics*. University of Southampton.

Timoshenko, S. P. (1965). *Strength of Materials- Part I.* (Stanford University, Ed.) (3th Edition).

Tsai, S. W., & Wu, E. M. (1971). A General Theory of Strength for Anisotropic Materials. *Journal of Composite Materials*, *5*(January), 58–80.